1991-12

# Higher order parametric x-rays

Osborne, Michael James

Monterey, California. Naval Postgraduate School

# NAVAL POSTGRADUATE SCHOOL
## Monterey, California


# THESIS

Higher Order Parametric X-Rays

by

Michael James Osborne

December 1991

Thesis Advisor: Xavier K. Maruyama

Approved for public release; distribution is unlimited.

Higher Order Parametric X-Rays

by

Michael J. Osborne
Lieutenant, United States Navy
B.S., The Citadel

Submitted in partial fulfillment
of the requirements for the degree of

MASTER OF SCIENCE IN PHYSICS

from the

NAVAL POSTGRADUATE SCHOOL
December 1991

Karlheinz E. Woehler, Chairman
Department of Physics

# REPORT DOCUMENTATION PAGE

Form Approved
OMB No 0704-0188

| | |
|---|---|
| 1a REPORT SECURITY CLASSIFICATION<br>Unclassified | 1b RESTRICTIVE MARKINGS |
| 2a SECURITY CLASSIFICATION AUTHORITY | 3 DISTRIBUTION / AVAILABILITY OF REPORT<br>Approved for public release; distribution is unlimited. |
| 2b DECLASSIFICATION / DOWNGRADING SCHEDULE | |
| 4 PERFORMING ORGANIZATION REPORT NUMBER(S) | 5 MONITORING ORGANIZATION REPORT NUMBER(S) |
| 6a NAME OF PERFORMING ORGANIZATION<br>Naval Postgraduate School<br>6b OFFICE SYMBOL (If applicable)<br>33 | 7a NAME OF MONITORING ORGANIZATION<br>Naval Postgraduate School |
| 6c ADDRESS (City, State, and ZIP Code)<br>Monterey, CA 93943-5000 | 7b ADDRESS (City, State, and ZIP Code)<br>Monterey, CA 93943-5000 |
| 8a NAME OF FUNDING / SPONSORING ORGANIZATION<br>8b OFFICE SYMBOL (If applicable) | 9 PROCUREMENT INSTRUMENT IDENTIFICATION NUMBER |
| 8c ADDRESS (City, State, and ZIP Code) | 10 SOURCE OF FUNDING NUMBERS<br>PROGRAM ELEMENT NO / PROJECT NO / TASK NO / WORK UNIT ACCESSION NO |

11 TITLE (Include Security Classification)

Higher Order Parametric X-Rays

12 PERSONAL AUTHOR(S)

Osborne, Michael J.

| 13a TYPE OF REPORT | 13b TIME COVERED | 14 DATE OF REPORT (Year, Month, Day) | 15 PAGE COUNT |
|---|---|---|---|
| Master's Thesis | FROM _____ TO _____ | December 1991 | 103 |

16 SUPPLEMENTARY NOTATION

The views expressed in this thesis are those of the author and do not reflect the official policy or position of the Department of Defense or the U.S. Government.

| 17 COSATI CODES | | | 18 SUBJECT TERMS (Continue on reverse if necessary and identify by block number) |
|---|---|---|---|
| FIELD | GROUP | SUB-GROUP | Parametric X-rays, PXR, Higher Order PXR, Easy-Mover |
| | | | |
| | | | |

19 ABSTRACT (Continue on reverse if necessary and identify by block number)

Parametric x-radiation (PXR) may be described as the Bragg scattering of virtual photons to produce real x-rays which satisfy the Bragg condition $d\sin_{\theta}=n\lambda$, where $_{\theta}$ is the angle between the electron beam direction and a crystal axis. Enhanced higher order parametric x-radiation from the {002} plane of a mosaic graphite crystal has been observed. Production of PXR of the order n=2 exceed that from the first order, and x-rays of order up to n=6 are readily seen. The production of higher order x-radiation is obtained by using a thick crystal where the formation and attenuation lengths are exploited to enhance higher energy x-ray formation relative to the lower energy first order x-radiation. Photons of energy 5 to 30 KeV have been measured. The experiment was conducted with a 90 MeV electron beam from the Naval Postgraduate School electron linear accelerator. A three axis target position program, Easy-Mover, was developed to allow for precision orientation of the crystal axis with respect to the electron beam.

| 20 DISTRIBUTION / AVAILABILITY OF ABSTRACT | 21 ABSTRACT SECURITY CLASSIFICATION |
|---|---|
| ☒ UNCLASSIFIED/UNLIMITED ☐ SAME AS RPT ☐ DTIC USERS | UNCLASSIFIED |
| 22a NAME OF RESPONSIBLE INDIVIDUAL<br>X.K. Maruyama | 22b TELEPHONE (Include Area Code)<br>(408)646-2431<br>22c OFFICE SYMBOL<br>Ph/Mx |

DD Form 1473, JUN 86 *Previous editions are obsolete*

S/N 0102-LF-014-6603

SECURITY CLASSIFICATION OF THIS PAGE
UNCLASSIFIED

## Abstract

Parametric x-radiation (PXR) may be described as the Bragg scattering of virtual photons to produce real x-rays which satisfy the Bragg condition $d\sin_{\theta}=n\lambda$, where $\theta$ is the angle between the electron beam direction and a crystal axis. Enhanced higher order parametric x-radiation from the {002} plane of a mosaic graphite crystal has been observed. Production of PXR of the order n=2 exceed that from the first order, and x-rays of order up to n=6 are readily seen. The production of higher order x-radiation is obtained by using a thick crystal where the formation and attenuation lengths are exploited to enhance higher energy x-ray formation relative to the lower energy first order x-radiation. Photons of energy 5 to 30 KeV have been measured. The experiment was conducted with a 90 MeV electron beam from the Naval Postgraduate School electron linear accelerator. A three axis target position program, Easy-Mover, was developed to allow for precision orientation of the crystal axis with respect to the electron beam.

## TABLE OF CONTENTS

I. INTRODUCTION.....1

II. THEORETICAL BACKGROUND.....2

III. EXPERIMENTAL PROCEDURE.....8

A. PXR EXPERIMENT.....8

B. PEAK INTENSITY RATIOS.....37

C. ROCKING DATA.....49

D. PXR EXPERIMENTAL SETUP.....58

E. LINAC TUNEUP PROCEDURE.....59

F. PULSE HEIGHT ANALYSIS PROCEDURE.....60

V. CONCLUSION AND RECOMMENDATIONS.....62

APPENDIX: EASY-MOVER PROGRAM.....64

A. INITIAL SUBROUTINE.....64

B. MAIN SCREEN.....65

C. ROTATION SUBSCREEN.....65

D. TILT SUBSCREEN.....67

E. HEIGHT SUBSCREEN.....68

F. INTERACTIVE PROGRAM.....69

G. EASY-MOVER COMPUTER PROGRAM.....70

LIST OF REFERENCES.....96

INITIAL DISTRIBUTION LIST.....98

# I. INTRODUCTION

Science has been searching for a monochromatic and intense x-radiation source. This search has led to the study of relativistic particles and their pseudo-photons in various media. [Ref 1] Parametric x-radiation (PXR) is formed by a relativistic particle interacting with the crystalline planes of a structure at or near the Bragg or Laue condition. Ter-Mikaelian first theorized this phenomena as resonant radiation in 1972 [Ref 2]. The first experiment verifying PXR was in 1985 at the Tomsk synchrotron by Baryshevsky et al [Ref. 3]. A diamond crystal was bombarded by 900 MeV electrons at a Bragg angle of 45 degrees producing PXR in the 5-25 keV range.

The Naval Postgraduate School experiment is the first measurement of PXR outside of the USSR. The PXR source for the experiment described in this thesis is a mosaic carbon crystal manufactured by Union Carbide. A subsequent thesis will present the data taken with a silicon crystal.

The measurements in this thesis show enhancement of higher order PXR due to the x-ray formation and attenuation within a thick crystal. To facilitate the acquisition of data, a three axis motor control program, Easy-Mover, described in the Appendix was developed.

## II. THEORETICAL BACKGROUND

Parametric x-radiation (PXR) is part of a larger class of radiation production mechanisms which include transition radiation (TR) and diffraction radiation (DR). When a charged particle beam satisfies the Bragg condition with the crystal lattice, the virtual photons associated with the relativistic particles are diffracted. PXR is produced when the periodic electric susceptability associated with the crystal lattice structure interacts with the field of the particle. [Ref 3]

The periodic lattice structure of the crystal leads to the diffraction of x-radiation photons with the wave vector $\kappa_B$ which satisfies the Bragg condition

$$\vec{\kappa}_B + \vec{\tau} = \vec{\kappa}' \quad where \quad |\vec{\kappa}'| = |\vec{\kappa}_B| \tag{1}$$

where $\tau$ is the reciprocal lattice vector. In the range of x-radiation, the refractive index $n(\kappa,\omega)$ becomes greater than unity and the Vavilov-Cherenkov radiation requirement,

$$1 - \frac{\vec{\kappa}\cdot\vec{v}}{\omega} n(\vec{\kappa},\omega) = 0, \qquad (\hbar = c = 1) \tag{2}$$

is satisfied even though the crystal dielectric constant $\epsilon$ is less than one. PXR originates when both the Bragg and Vavilov-Cherenkov conditions are satisfied by the wave vector

$\kappa$ and the frequency $\omega$ of the emitted photons generated by the charged particle moving through the lattice structure of a crystal with uniform velocity. [Ref 2] In contrast to the crystal structure, homogeneous media require that the refractive index n is less than one for the production of x-radiation, demonstrating that under the Bragg diffraction condition the Vavilov-Cherenkov radiation is PXR.

The kinematic theory of PXR is applicable for crystals which consist of thin mosaic blocks with angle of $\delta > m/E$ relative to each other where m is the mass of the beam particle and E is its energy. Ter-Mikaelian formulated the number of photons emitted by a charged particle in a thin crystal treating the interaction as a perturbation with the crystal requirement

$$\kappa L \mid n-1 \mid < 1 \qquad (3)$$

where L is the thickness of the crystal. If the refraction of photons and the multiple scattering of electrons in the crystal are accounted for, the results for a mosaic crystal meeting the crystal requirement whose PXR from different blocks are incoherent remain correct. The spectral and angular distributions of emitted photons are formulated by

$$\frac{\partial^2 N}{\partial \overline{n}_\perp \partial \omega} = \frac{e^2}{2\pi} \omega L_a |g_\tau|^2 \frac{|[\overline{K}_\perp, \omega\overline{v}+\overline{\tau}]|^2}{\left[(\overline{K}_\perp-\overline{\tau}_\perp)^2 + \frac{\omega^2}{v^2}(1-v^2)\right]^2} \quad (4)$$

$$\times\left[1-e^{\left(-\frac{L}{L_a}\right)}\right]\delta(q);$$

$$q = \frac{\omega}{v} - \sqrt{\omega^2 - K_\perp^2} + \tau_z - \frac{\omega}{2}\left[Re(g_o) - \theta_s^2\right]; \quad (5)$$

$$\theta_s = \frac{E_s}{E}\sqrt{\frac{L}{L_R}}. \quad (6)$$

The Fourier components of the dielectric susceptibility corresponding to the reciprocal lattice vector $g_E$ and the mean value $g_o$ are directly connected with the coherent scattering amplitude of the photons; $\theta_s$ is the angle of multiple scattering; $E_s \cong 21$ MeV and $L_R$ is the radiation length. The particle velocity $v$ is directed along the z-axis; $K_z = \omega n_\perp$; and $L_a = [\omega\ \mathrm{Im}\ (g_o)]^{-1}$ is the absorption length for x-radiation in the crystal. [Ref 4]

The characteristic of producing the quasi-monochromatic photons at large angles to the velocity vector $v$ distinguishes PXR from other radiation mechanisms. The particle energy does not determine the emitted photon wave vectors $K_B$ and their frequencies $\omega_B$. They are defined by the reciprocal lattice vectors $\tau$ and the angle $\theta_B$ between the

vector $v$ and crystallographic planes connected with the vectors $\tau$. The PXR maxima are defined by the crystal lattice structure amplitudes corresponding to the vectors $\tau$. The values for the emitted wave vectors $\kappa_B$ and their frequencies $\omega_B$ are

$$2\theta_B = \frac{\overline{\kappa}_B \cdot \overline{v}}{\omega_B} \tag{7}$$

$$\omega_B(n) = \frac{\tau}{2|\tau_z|} = \frac{\tau}{2\sin\theta_B} = \frac{\pi n}{d\sin\theta_B} \quad n = 1, 2 \ldots \tag{8}$$

where d is the distance between the crystal planes corresponding to the vector $\tau$. [Ref 2]

The intensity of PXR is proportional to $|g_E|^2$ therefore it is greater in crystals with higher packing factors, such as a diamond lattice. Rotation of the crystal by some $\Delta\theta$ results in the emitted wave vector $\kappa_B$ rotating $2\Delta\theta$ in the same direction while the frequency varies by the above formula. The angular distribution of emitted photons can be derived from the formula for the spectral and angular distribution by integrating over $\omega$, resulting in

$$\frac{\partial^2 N}{\partial\theta_x \partial\theta_y} = \sum_{n=1}^{\infty} \frac{e^2}{4\pi}\omega_B L_a\left[1 - e^{\left(-\frac{L}{L_a}\right)}\right] \frac{|g_\tau(\omega_B)|^2}{\sin^2\theta_B} \frac{\left[\theta_x^2 \cos^2 2\theta_B + \theta_y^2\right]}{\left[\theta_x^2+\theta_y^2+\theta_{ph}^2\right]^2}; \quad (9)$$

$$\theta_{x,y} = \frac{(K - K_B)_{x,y}}{\omega_B}; \quad \theta_{ph}^2 = \frac{m^2}{E^2} + \theta_s - |g_o|, \quad (10)$$

where m is the rest mass of the electron.

The number of photons detected over an angular distribution of $\theta_d$ about the Bragg angle is given by

$$N_d = \pi N_o(1+\cos^2\theta_B)\int_0^{\rho_d} \frac{\rho^3 d\rho}{(\rho^2+1)^2}$$

$$= N_1(1+\cos^2 2\theta_B)\ln\left[\frac{\theta_d^2+\theta_{ph}^2}{\theta_{ph}^2} - \frac{\theta_d^2}{\theta_d^2+\theta_{ph}^2}\right]; \quad (11)$$

$$\text{where } \rho_d = \frac{\theta_d}{\theta_{ph}}.$$

The detection angular size is a factor in determining the value of $N_d$ even for $\theta_d \ll \theta_{ph}$. This factor does not appear in channeling and bremsstrahlung radiation, however in PXR the intensity slowly decreases as $\theta$ increases.

The angular distribution as defined by the parameter $\theta_{ph}(E)$ increases for the electron energy

$$E < E_{opt} = \sqrt{\frac{m^2 + E_s^2 \frac{L}{L_R}}{|Re\, g_o|}} \qquad (12)$$

setting the limiting threshold energy for PXR. The amount of photons detected decreases rapidly for $E < E_{opt}$. The number detected becomes

$$N_D = \frac{\pi}{2} N_o (1 + \cos^2 2\theta_B) \frac{1}{2} \left( \frac{\theta_D}{\theta_{ph}} \right)^4 \sim \left( \frac{E}{E_{opt}} \right)^4 . \qquad (13)$$

This phenomena illustrates the problem that, even if all other parameters are met, if the energy of the particle beam is not high enough, PXR may not be detectable. [Ref 4]

## III. PXR EXPERIMENT

The PXR experiment was conducted with two separate goals. The first goal was to determine the intensity ratios of the higher order peaks to the intensity of the first order peak. In this experiment we have made the first observation of enhanced higher order Bragg peaks. The data were taken at Bragg angles of 22.5 and 21.7 degrees and are presented in the Peak Intensities Ratios subsection. The second part of the experiment dealt with the energy of the peaks. The energy of the different peaks were compared with each other for each Bragg angle. The first peak energy was evaluated as the crystal was rotated to each Bragg angle.

### A. PXR EXPERIMENT

The PXR experiment was conducted at the NPS linac with dark current tuned to an energy of 90 MeV. The dark current was not able to be accurately measured, however the current is estimated to be less than $10^{-10}$ amperes.

Figure 1 represents the arrangement of the crystal and scattering chamber. A mosaic carbon crystal is located on the ladder at the center of the scattering chamber. The mosaic carbon crystal is a graphite monochromator manufactured by Union Carbide. The spacing of the reflecting <002> planes is 3.353 to 3.359 angstroms. The mosaic spread is greater than

or equal to 0.4 degrees and the density is 2.255 to 2.265 grams per cubic centimeter. The thickness of the crystal is 2.0 millimeters with a zero millimeter plus tolerance and a 1.0 millimeter minus tolerance. The reference laser location defines the zero angle position with the electron beam at 270 degrees and the SiLi detector at 45 degrees.

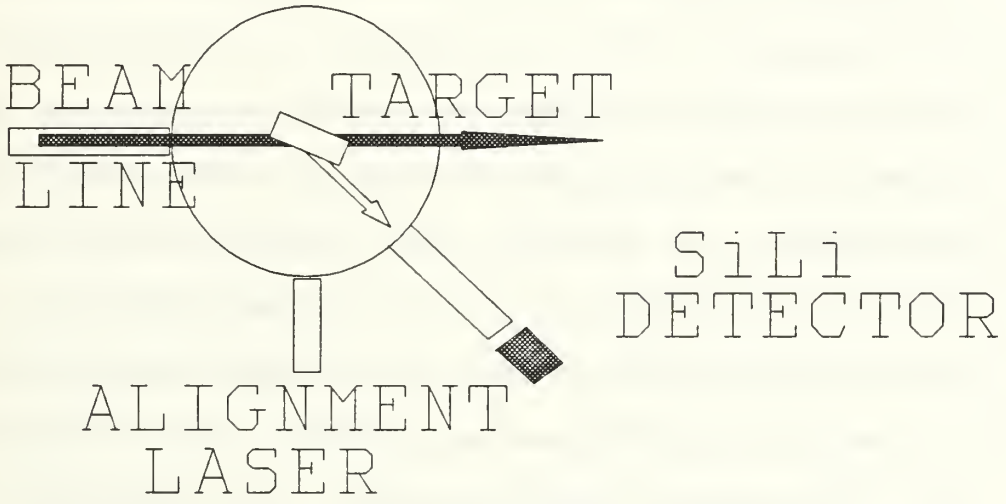


Figure 1: The arrangement of the scattering chamber.

We have developed an unique method for x-ray energy calibration in the accelerator end station environment which is plagued by klystron RF noise. The RF distorts the energy calibration during the period the klystrons are pulsed. Therefore, energy calibrations must be made during the on-time

of the accelerator which is 60 pulses of one microsecond duration per second. A phosphorescent view screen was backed with strips of titanium and copper. When the electron beam struck the view screen, the titanium and copper atoms were excited. The SiLi detector then observed the $k_\alpha$ x-rays of de-excitation. The $k_\alpha$ x-rays are observed at 8.05 KeV for copper and 4.5 KeV for titanium [Ref. 5]. The calibration peaks have a full width at half maximum of 34 channels corresponding to an energy resolution of 1.06 KeV. This energy resolution contributes to the uncertainty in determining the PXR radiation peaks' energy. We estimate that we are able to determine x-ray energies to 200 eV. The calibration data consequently is observed only during the time when the electron impinges on the target and sees the same RF environment as the PXR from the mosaic carbon target.

Once the calibration was achieved, the ladder height was set at the mosaic carbon crystal. The reference laser beam was reflected from the target crystal oriented at zero degrees back to the laser. From the reference position, the target was rotated to the desired Bragg angle. To achieve a Bragg angle of 22.5 degrees, the target was rotated counter-clockwise 157.5 degrees from the reference orientation. The data initially taken at $\theta_B$ = 22.5 degrees is presented in Table 1, Figure 3 and Figure 4.

After the data for the Bragg angle of 22.5 degrees was taken, the ladder was rotated in a counter-clockwise rotation

at steps of 0.2 degrees to observe the count rate in a PXR peak as a function of the Bragg angle. The peaks were monitored for count rate and at 21.7 degrees the highest count rate was observed, so data was taken at this Bragg angle. The angle of the SiLi detector remained at 45 degrees relative to the electron beam line. Figure 5, Figure 6 and Table 2 show the data for the Bragg angle of 21.7 degrees. Note that for both the $\theta_B$ = 22.5 and 21.7 degrees, the measured integer ratio E(n)/E(1) satisfies the Bragg relation, equation (8).

Next the target was returned to the reference angle and then set to an angle of 156.0 degrees counter-clockwise from the reference, corresponding to a Bragg angle of 24.0 degrees. Data was taken for this angle, and for the target rotated through to the Bragg angles 23.0, 22.5, 22.0, 21.5, 21.0, 20.0 and 19.0 degrees. This data is presented in Figures 7 to 14 and Tables 3 to 10. The highest count rate for this set of data was obtained for a Bragg angle of 21.5 degrees.

The data taking rate was limited by the detector system which could detect at most one photon per beam pulse. Even at a Bragg angle of 21.7 degrees where the number of counts was the highest the peak $\Delta n/n$ was never below 4.6 % even though the data was taken for 1.5 hours. The integrations of the area by the PHA program resulted in evaluations of the data that were three to four times better statistically in $\Delta n/n$. Taking the full width half maximum times the peak value

brought in the uncertainties from the FWHM to compound those for the peak value.

Several methods exist to evaluate the area under the peak. Due to the poor statistics, the method used for the rotating angles of 19.0 to 24.0 degrees required some judgement. The edge of the peaks were evaluated by estimating the background and setting the region of interest based on the perceived background. This method was useful for peaks where the total number of counts were very low.

The method used in the 22.5 and 21.7 degree Bragg angles involved a more systematic approach. First, the peak maximum channel was determined and then the edge of the peak was estimated. Locating the edge of the first and second peaks for angles with many counts was straight forward. Next, the number of channels to the edge of the first peak was noted and used to determine the width of every peak in the spectrum. If the first peak had a base width of 80 channels then 80 channels were used for all the other peaks. The center of the channels were determined by the location of the maximum peak channel and then the number of channels were counted out to both sides of the peak. After the peaks were evaluated the background levels between the peaks were set as a region of interest to obtain the total number of counts in that background region. Next, to determine the number of counts per channel in the background, the total number of counts were divided by the number of channels. Once the background level

was determined in this fashion, the results were compared to the background evaluated in the peak.

Figure 2: PXR spectrum for the Ti-Cu calibration with a 90 MeV beam. The Ti peak is at 4.5 KeV and Cu peak is at 8.05 KeV.

TABLE 1: MOSAIC CARBON CRYSTAL {002} PLANE PEAK DATA FOR 90 MeV ELECTRON BEAM AT A BRAGG ANGLE OF $\theta_B$ = 22.5 DEGREES.

| Peak # | 1 | 2 | 3 | 4 | 5 | 6 |
|---|---|---|---|---|---|---|
| Peak Chl | 245 | 407 | 576 | 731 | * | * |
| Energy KeV | 5.3 | 10.4 | 15.7 | 20.6 | * | * |
| E(n)/E(1) | 1.0 | 1.96 | 2.96 | 3.89 | * | * |
| CTRD Chl | 241.9 | 405.5 | 573.3 | 731.4 | * | * |
| FWHM Chl | 28.2 | 30.7 | 44.6 | 72.3 | * | * |
| Peak Gross | 314 | 243 | 119 | 63 | * | * |
| Peak Bkgnd | 39 | 41 | 40 | 34 | * | * |
| Peak Net | 275 | 202 | 79 | 29 | * | * |
| Peak $\Delta$n/n% | 6.8 | 8.3 | 16.0 | 34.0 | * | * |
| Area Gross | 9560 | 8228 | 4840 | 3166 | * | * |
| Area Bkgnd | 2769 | 2911 | 2840 | 2414 | * | * |
| Area Net | 6791 | 5317 | 2000 | 652 | * | * |
| Area $\Delta$n/n% | 1.6 | 2.0 | 4.4 | 11.4 | * | * |
| Net Cts/s | 0.6642 | 0.5201 | 0.1956 | 0.0638 | * | * |

Figure 3: PXR spectrum for a Bragg angle of 22.5 degrees and a 90 MeV beam.

Figure 4: PXR spectrum, log scale, for a Bragg angle of 22.5 degrees and a 90 MeV beam.

TABLE 2: MOSAIC CARBON CRYSTAL {002} PLANE PEAK DATA FOR 90 MeV ELECTRON BEAM AT A BRAGG ANGLE OF $\theta_B$ = 21.7 DEGREES.

| Peak # | 1 | 2 | 3 | 4 | 5 | 6 |
|---|---|---|---|---|---|---|
| Peak Chl | 233 | 390 | 553 | 712 | 876 | 1054 |
| Energy KeV | 5.0 | 9.9 | 15.0 | 20.0 | 25.2 | 30.8 |
| E(n)/E(1) | 1.0 | 1.98 | 3.0 | 3.5 | 5.04 | 6.16 |
| CTRD Chl | 232.4 | 389.9 | 551.5 | 713.2 | 876.6 | 1051.8 |
| FWHM Chl | 17.0 | 20.0 | 22.0 | 20.7 | 34.8 | 77.7 |
| Peak Gross | 501 | 567 | 264 | 115 | 55 | 36 |
| Peak Bkgnd | 28 | 22 | 20 | 19 | 15.2 | 14 |
| Peak Value | 473 | 545 | 244 | 96 | 39.8 | 22 |
| Peak $\Delta$n/n% | 4.9 | 4.6 | 6.9 | 12.1 | 21.1 | 32.1 |
| Area Gross | 10635 | 12861 | 6823 | 3569 | 2132 | 1517 |
| Area Bkgnd | 2268 | 1782 | 1620 | 1539 | 1215 | 1134 |
| Area Net | 8367 | 11079 | 5203 | 2030 | 917 | 383 |
| Area $\Delta$n/n% | 1.4 | 1.1 | 1.8 | 3.5 | 6.3 | 13.4 |
| Net Cts/sec | 1.412 | 1.869 | 0.878 | 0.343 | 0.155 | 0.065 |

Figure 5: PXR spectrum for a Bragg angle of 21.7 degrees with a 90 MeV beam.

Figure 6: PXR spectra, log scale, for a Bragg angle of 21.7 degrees with a 90 MeV beam.

TABLE 3: MOSAIC CARBON CRYSTAL {002} PLANE PEAK DATA FOR 90 MeV ELECTRON BEAM AT A BRAGG ANGLE OF $\theta_B$ = 19.0 DEGREES.

| Peak # | 1 | 2 | 3 | 4 | 5 | 6 |
|---|---|---|---|---|---|---|
| Peak Chl | 222 | 350 | 528 | * | * | * |
| Energy KeV | 1.0 | 8.6 | 14.2 | * | * | * |
| E(n)/E(1) | 1.0 | 1.87 | 3.09 | * | * | * |
| CTRD Chl | 223.8 | 355.5 | 530.9 | * | * | * |
| FWHM Chl | 28.3 | 9.7 | 13.0 | * | * | * |
| Peak Gross | 8 | 7 | 5 | * | * | * |
| Peak Bkgnd | 2 | 1 | 1 | * | * | * |
| Peak Value | 6 | 6 | 4 | * | * | * |
| Peak $\Delta$n/n% | 52.7 | 47.1 | 61.2 | * | * | * |
| Area Gross | 136 | 1 | 28 | * | * | * |
| Area Bkgnd | 78 | 31 | 20 | * | * | * |
| Area Net | 58 | 35 | 8 | * | * | * |
| Area $\Delta$n/n% | 25.2 | 23.0 | 86.6 | * | * | 6 |
| Net Cts/s | 0.170 | 0.102 | 0.024 | * | * | * |

Figure 7: PXR spectrum for a Bragg angle of 19.0 degrees and a 90 MeV beam.

TABLE 4: MOSAIC CARBON CRYSTAL {002} PLANE PEAK DATA FOR 90 MeV ELECTRON BEAM AT A BRAGG ANGLE OF $\theta_B$ = 20.0 DEGREES.

| Peak # | 1 | 2 | 3 | 4 | 5 | * |
|---|---|---|---|---|---|---|
| Peak Chl | 224 | 372 | 565 | 677 | * | * |
| Energy KeV | 4.7 | 9.3 | 15.4 | 18.9 | * | * |
| E(n)/E(1) | 1.0 | 1.98 | 3.28 | 4.02 | * | * |
| CTRD Chl | 223.8 | 374.2 | 565.4 | 674.6 | * | * |
| FWHM Chl | 20.5 | 16.3 | 13.5 | 19.3 | * | * |
| Peak Gross | 13 | 10 | 6 | 5 | * | * |
| Peak Bkgnd | 1 | 1 | 1 | 1 | * | * |
| Peak Value | 12 | 9 | 5 | 1 | * | * |
| Peak $\Delta$n/n% | 31.2 | 36.9 | 52.9 | 61.2 | * | * |
| Area Gross | 195 | 162 | 36 | 45 | * | * |
| Area Bkgnd | 39 | 38 | 23 | 31 | * | * |
| Area Net | 156 | 124 | 13 | 14 | * | * |
| Area $\Delta$n/n% | 9.8 | 11.4 | 59.1 | 62.2 | * | * |
| Net Cts/s | 0.502 | 0.399 | 0.042 | 0.045 | * | * |

Figure 8: PXR spectrum for a Bragg angle of 20.0 degrees and a 90 MeV beam.

TABLE 5: MOSAIC CARBON CRYSTAL {002} PLANE PEAK DATA FOR 90 MeV ELECTRON BEAM AT A BRAGG ANGLE OF $\theta_B$ = 21.0 DEGREES.

| Peak # | 1 | 2 | 13 | 1 | 5 | 6 |
|---|---|---|---|---|---|---|
| Peak Chl | 226 | 373 | 538 | 690 | * | * |
| Energy KeV | 9.0 | 9.4 | 14.5 | 19.3 | * | * |
| E(n)/E(1) | 1.0 | 1.96 | 3.02 | 4.02 | * | * |
| CTRD Chl | 224.2 | 373.7 | 529.1 | 691.5 | * | * |
| FWHM Chl | 9.0 | 28.0 | 23.2 | 25.3 | * | * |
| Peak Gross | 20 | 13 | 7 | 6 | * | * |
| Peak Bkgnd | 1 | 1 | 1 | 1 | * | * |
| Peak Value | 19 | 12 | 6 | 5 | * | * |
| Peak $\Delta$n/n% | 24.1 | 31.2 | 47.1 | 52.9 | * | * |
| Area Gross | 255 | 202 | 12 | 77 | * | * |
| Area Bkgnd | 38 | 34 | 34 | 43 | * | * |
| Area Net | 217 | 168 | 13 | 43 | * | * |
| Area $\Delta$n/n% | 7.9 | 9.4 | 22.4 | 32.2 | * | * |
| Net Cts/s | 0.670 | 0.519 | 0.148 | 0.133 | * | * |

Figure 9: PXR spectrum for a Bragg angle of 21.0 degrees and a 90 MeV beam.

TABLE 6: MOSAIC CARBON CRYSTAL {002} PLANE PEAK DATA FOR 90 MeV ELECTRON BEAM AT A BRAGG ANGLE OF $\theta_B$ = 21.5 DEGREES.

| Peak # | 1 | 2 | 3 | 4 | 5 | * |
|---|---|---|---|---|---|---|
| Peak Chl | 233 | 388 | 541 | 700 | 863 | * |
| Energy KeV | 5.0 | 9.8 | 14.6 | 19.6 | 24.8 | * |
| E(n)/E(1) | 1.0 | 1.96 | 2.92 | 3.92 | 4.96 | * |
| CTRD Chl | 229.2 | 384.3 | 544.1 | 705.4 | 869.5 | * |
| FWHM Chl | 13.4 | 16.4 | 23.7 | 29.2 | 18.6 | * |
| Peak Gross | 47 | 53 | 19 | 42 | 5 | * |
| Peak Bkgnd | 1 | 1 | 1 | 1 | 1 | * |
| Peak Value | 46 | 52 | 19 | 11 | 1 | * |
| Peak $\Delta$n/n% | 15.1 | 14.1 | 24.8 | 32.8 | 61.2 | * |
| Area Gross | 630 | 843 | 364 | 154 | 60 | * |
| Area Bkgnd | 52 | 52 | 37 | 42 | 33 | * |
| Area Net | 638 | 791 | 327 | 112 | 27 | * |
| Area $\Delta$n/n% | 4.3 | 3.8 | 9.8 | 12.5 | 35.7 | * |
| Net Cts/s | 1.849 | 2.293 | 0.948 | 0.325 | 0.078 | * |

Figure 10: PXR spectrum for a Bragg angle of 21.5 degrees and a 90 MeV beam.

TABLE 7: MOSAIC CARBON CRYSTAL {002} PLANE PEAK DATA FOR 90 MeV ELECTRON BEAM AT A BRAGG ANGLE OF $\theta_B$ = 22.0 DEGREES.

| Peak # | 1 | 2 | 3 | 3 | 5 | 6 |
|---|---|---|---|---|---|---|
| Peak Chl | 229 | 388 | 551 | 724 | 892 | 1035 |
| Energy KeV | 1.0 | 9.8 | 14.6 | 20.4 | 25.7 | 30.2 |
| E(n)/E(1) | 1.0 | 2.04 | 3.04 | 4.25 | 5.35 | 6.29 |
| CTRD Chl | 231.8 | 388.4 | 549.5 | 717.4 | 884.6 | 1042.2 |
| FWHM Chl | 16.8 | 12.8 | 29.8 | 21.7 | 36.9 | 19.6 |
| Peak Gross | 25 | 40 | 14 | 8 | 1 | 5 |
| Peak Bkgnd | 1 | 2 | 1 | 1 | 1 | 4 |
| Peak Value | 24 | 40 | 13 | 8 | 3 | 4 |
| Peak $\Delta$n/n% | 21.2 | 17.1 | 29.8 | 17.1 | 74.5 | 61.2 |
| Area Gross | 416 | 528 | 249 | 101 | 71 | 35 |
| Area Bkgnd | 33 | 76 | 40 | 31 | 47 | 31 |
| Area Net | 383 | 452 | 209 | 76 | 24 | 4 |
| Area $\Delta$n/n% | 5.5 | 5.4 | 5.4 | 16.4 | 45.3 | 203.1 |
| Net Cts/s | 1.570 | 1.852 | 0.857 | 0.287 | 0.098 | 0.016 |

Figure 11: PXR spectrum for a Bragg angle of 22.0 degrees and a 90 MeV beam.

TABLE 8: MOSAIC CARBON CRYSTAL {002} PLANE PEAK DATA FOR 90 MeV ELECTRON BEAM AT A BRAGG ANGLE OF $\theta_B$ = 22.5 DEGREES.

| Peak # | 1 | 2 | 3 | 4 | 5 | 6 |
|---|---|---|---|---|---|---|
| Peak Chl | 231 | 391 | 554 | 723 | * | * |
| Energy KeV | 4.9 | 9.9 | 15.1 | 20.4 | * | * |
| E(n)/E(1) | 1.0 | 2.02 | 3.08 | 4.16 | * | * |
| CTRD Chl | 232.2 | 390.0 | 553.3 | 715.6 | * | * |
| FWHM Chl | 11.2 | 17.2 | 23.6 | 18.8 | * | * |
| Peak Gross | 23 | 24 | 11 | 7 | * | * |
| Peak Bkgnd | 1 | 1 | 1 | 1 | * | * |
| Peak Value | 22 | 23 | 10 | 6 | * | * |
| Peak $\Delta$n/n% | 22.3 | 21.7 | 34.6 | 47.1 | * | * |
| Area Gross | 303 | 378 | 148 | 62 | * | * |
| Area Bkgnd | 61 | 48 | 38 | 32 | * | * |
| Area Net | 242 | 330 | 140 | 30 | * | * |
| Area $\Delta$n/n% | 7.9 | 6.3 | 12.4 | 32.3 | * | * |
| Net Cts/s | 1.034 | 1.410 | 0.470 | 0.128 | * | * |

Figure 12: PXR spectrum for a Bragg angle of 22.5 degrees and a 90 MeV beam.

TABLE 9: MOSAIC CARBON CRYSTAL {002} PLANE PEAK DATA FOR 90 MeV ELECTRON BEAM AT A BRAGG ANGLE OF $\theta_B$ = 23.0 DEGREES.

| Peak # | 1 | 2 | 3 | 4 | 5 | * |
|---|---|---|---|---|---|---|
| Peak Chl | 235 | 399 | 564 | 723 | * | * |
| Energy KeV | 5.0 | 10.2 | 15.4 | 20.4 | * | * |
| E(n)/E(1) | 1.0 | 2.04 | 3.08 | 4.08 | * | * |
| CTRD Chl | 235.6 | 397.0 | 561.3 | 719.2 | * | * |
| FWHM Chl | 14.2 | 25.4 | 27.8 | 15.8 | * | * |
| Peak Gross | 14 | 11 | 8 | 5 | * | * |
| Peak Bkgnd | 2 | 2 | 1 | 1 | * | * |
| Peak Value | 12 | 9 | 8 | 4 | * | * |
| Peak $\Delta$n/n% | 33.3 | 40.1 | 47.1 | 61.2 | * | * |
| Area Gross | 201 | 1[illegible]2 | 78 | 35 | * | * |
| Area Bkgnd | 70 | 66 | 31 | 18 | * | * |
| Area Net | 131 | 108 | 47 | 17 | * | * |
| Area $\Delta$n/n% | 12.5 | 14.3 | 22.2 | 42.8 | * | * |
| Net Cts/s | 0.435 | 0.359 | 0.156 | 0.057 | * | * |

Figure 13: PXR spectrum for a Bragg angle of 23.0 degrees with a 90 MeV beam.

TABLE 10: MOSAIC CARBON CRYSTAL {002} PLANE PEAK DATA FOR 90 MeV ELECTRON BEAM AT A BRAGG ANGLE OF $\theta_B$ = 24.0 DEGREES.

| Peak # | 1 | 2 | * | * | 5 | 6 |
|---|---|---|---|---|---|---|
| Peak Chl | 239 | 401 | * | * | * | * |
| Energy KeV | 5.2 | 10.2 | * | * | * | * |
| E(n)/E(1) | 1.0 | 1.96 | * | * | * | * |
| CTRD Chl | 240.5 | 405.3 | * | * | * | * |
| FWHM Chl | 18.0 | 21.3 | * | * | * | * |
| Peak Gross | 10 | 6 | * | * | * | * |
| Peak Bkgnd | 2 | 2 | * | * | * | * |
| Peak Net | 8 | 4 | * | * | * | * |
| Peak $\Delta$n/n% | 43.3 | 70.7 | * | * | * | * |
| Area Gross | 123 | 75 | * | * | * | * |
| Area Bkgnd | 52 | 54 | * | * | * | * |
| Area Net | 71 | 21 | * | * | * | * |
| Area $\Delta$n/n% | 18.6 | 54.1 | * | * | * | * |
| Net Cts/s | 0.198 | 0.059 | * | * | * | * |

Figure 14: PXR spectrum for a Bragg angle of 24.0 degrees and a 90 MeV beam.

B. PEAK INTENSITY RATIOS

The intensity of the x-radiation is reduced by a transmission factor which is less than unity. The absorption length $L_a$ is dependent on the linear absorption coefficient $\mu$. Scofield's values for $\mu$ are used to determine $L_a$ for the mosaic carbon crystal: [Ref. 6]

$$\mu\left[\frac{cm^2}{g}\right]=\mu\left[\frac{barns}{atom}\right]\left[19.94\ \frac{cm^2}{g}\ \frac{atom}{barns}\right]; \tag{14}$$

$$\mu\left[\frac{1}{cm}\right]=\rho\left[\frac{g}{cm^3}\right]\mu\left[\frac{cm^2}{g}\right]=\frac{1}{L_a[cm]}; \tag{15}$$

$$where \quad \rho=2.25\left[\frac{g}{cm^3}\right]. \tag{16}$$

The absorption length $L_a$ for carbon is dependent on the energy of the x-radiation and is tabulated in Table 11.

One characteristic of PXR being studied was the relative intensities of the $n^{th}$ order peaks in relation to the first order intensity. Taking the factors in equation (9) that are variables of the order n of reflection in carbon, the intensity I(n) has the relationship,

$$I(n)\propto\omega_B(n)L_a\left[1-e^{-\frac{L}{L_a}}\right]|g_\tau(\omega_B(n))|^2 \tag{17}$$

$$g_t = \Gamma F_H(\theta, \lambda) \tag{18}$$

$$\Gamma = \frac{r_e \lambda^2}{\pi V} \tag{19}$$

where $F_H(\theta,\lambda)$ is the structure factor for x- radiation scattering; $r_e$ is the classical electron radius; V is the volume of the unit cell; and $\lambda$ is the wavelength of the x-radiation. The properties of the radiation which depend on n are:

$$\omega_B(n) = \frac{n\pi c}{d \sin \theta_B} \propto n \tag{20}$$

$$g_t \propto \frac{1}{\omega_B^2(n)} \propto \frac{1}{n^2}. \tag{21}$$

Equations (20) and (21) can be combined to give the relationship

$$\therefore \omega_B(n)\,|g_t(\omega_B(n))|^2 \propto \frac{1}{\omega_B^3(n)} \propto \frac{1}{n^3} \tag{22}$$

Therefore the intensity of the n $^{th}$ order peak with the absorption length $L_a$ taken into account is:

$$I(n) \propto \frac{L_a\left(1 - e^{-\frac{L}{L_a}}\right)}{n^3} \qquad (23)$$

The ratio I(n)/I(1) in Tables 13 and 14 is determined by the relationship:

$$\frac{I(n)}{I(1)} = \frac{1}{n^3}\,\frac{L_a(n)}{L_a(1)}\left[1 - e^{\left(\frac{-L}{L_a(n)}\right)}\right]. \qquad (24)$$

The absorption length $L_a$ is implicitly a function of n because it is energy dependent. If the crystal is sufficiently thick such that $L >> L_a$ equation (24) becomes: [Ref. 6]

$$\lim_{L\to\infty} \frac{I(n)}{I(1)} = \lim_{L\to\infty} \frac{1}{n^3}\,\frac{L_a(n)}{L_a(1)}\left[1 - e^{\left(\frac{-L}{L_a(n)}\right)}\right] = \frac{1}{n^3}\,\frac{L_a(n)}{L_a(1)}. \qquad (25)$$

The structure factor of graphite in our geometry is

$$F_H = 4f\left(\frac{\sin\theta}{\lambda}\right)\cos^2\left[\frac{\pi(h+2k)}{3}\right] \qquad l = even\ ; \qquad (26)$$

$$F_H = 2\,i\,f\left(\frac{\sin\theta}{\lambda}\right)\sin\left[\frac{2\pi(h+2k)}{3}\right] \qquad l = odd\ . \tag{27}$$

For the {002} planes, where h = k = 0 and l = even, the reflection structure factor becomes [Ref. 7]

$$F_H = 4\,f\left(\frac{\sin\theta}{\lambda}\right). \tag{28}$$

If the reflection structure factor is included in equation (24), the ratio of the intensities becomes

$$\frac{I(n)}{I(1)} = \frac{1}{n^3}\,\frac{L_a(n)}{L_a(1)}\left[1 - e^{\left(\frac{-L}{L_a(n)}\right)}\right]\frac{f(n)}{f(1)}\ . \tag{29}$$

After the PXR is generated, it must travel through a one mil Kapton window before reaching the SiLi detector which is not in a vacuum. The SiLi detector efficiency is also energy dependent. Table 12 lists the correction factors due to kapton window and air gap absorption and detector efficiency [Ref. 8]. The ratios of the theoretical and experimental intensities for Bragg angles of 22.5 and 21.7 degrees are tabulated in Tables 13 and 14 respectively.

Graphs 1 and 2 plot the intensity ratios for each of the peaks vs the peak number for the Bragg angles of 21.7 and 22.5 degrees respectively. The observed ratios are not self consistent nor consistent with theoretical calculations. The

experimental values closely follow the theoretical values of equation (24) for the Bragg angle of 21.7 degrees. When the structure factor is included in the theory the higher order experimental peak values drastically exceed those of the first peak that the theory predicts for a Bragg angle $\theta_B$ = 21.7 degrees. However in the plot of $\theta_B$ = 22.5 degrees, the experimental ratio are closer to those of equation (29) that include the structure factor. The structure factor "depends upon the scattering properties of the matter in the crystal [Ref. 9]".

In the case of a Bragg angle of 21.7 degrees the PXR may not have been centered within a three foot copper two inch diameter vacuum pipe from the scattering chamber to the detector. The target is located 17 inches from the edge of the scattering chamber. The detector could possibly be x-rays that are being reflected off the pipe walls. When the PXR is centered on the detector, as it should be in the $\theta_B$ = 22.5 degrees case, the data should be closer to the theoretically predicted value. At the Bragg angle of 22.5 degrees however the experimental values are still higher than the equation (29) curve. This phenomena could be explained if the reflecting off the port walls that might have occurred at 21.7 degrees still had an effect at 22.5 degrees. The reflection off the walls contribution would be smaller when the PXR is centered in the port than previously. This would lead to higher intensity ratios than the theory with the structure

factor, however not as high as was seen at a Bragg angle of 21.7 degrees. These explanations are still conjectural and need further investigation. Other causes might include non uniformity in the crystal thickness. A future experiment with a collimated detector placed close enough to the scattering chamber that would preclude this reflection could test the validity of this conjecture.

TABLE 11: SCOFIELD'S VALUES [REF. 5] FOR CARBON FOR THE LINEAR ABSORPTION COEFFICIENT $\mu$ AND THE ASSOCIATED ABSORPTION LENGTH $L_a$.

| $h\omega_B$ (KeV) | $\mu$ (barns/atom) | $\mu$ ($cm^2/g$) | $L_a$ (cm) |
|---|---|---|---|
| 5 | 385.9 | 19.35 | 0.0230 |
| 10 | 40.08 | 2.010 | 0.221 |
| 15 | 16.86 | 0.846 | 0.526 |
| 20 | 16.06 | 0.454 | 0.979 |
| 25 | 6.070 | 0.304 | 1.46 |
| 30 | 5.114 | 0.256 | 1.74 |

TABLE 12: CORRECTION FACTORS FOR MEDIA TRANSMISSION AND DETECTOR EFFICIENCY FOR INTENSITY VS ENERGY.

| Energy KeV | Kapton Trans-mission | 3 cm Air Trans-mission | Detector Efficiency | Product of factors | 1/product of factors |
|---|---|---|---|---|---|
| 5 | 0.915 | 0.864 | 1.0 | 0.791 | 1.265 |
| 10 | 0.990 | 0.979 | 1.0 | 0.990 | 1.056 |
| 15 | 0.996 | 0.864 | 1.0 | 0.990 | 1.011 |
| 25 | 1.0 | 1.0 | 0.97 | 0.97 | 1.031 |
| 25 | 1.0 | 1.0 | 0.86 | 0.86 | 1.162 |
| 30 | 1.0 | 1.0 | 0.72 | 0.72 | 1.400 |

TABLE 13: THEORETICAL AND EXPERIMENTAL VALUES FOR THE INTENSITY OF THE $n^{th}$ ORDER PEAK VS THE n = 1 PEAK AT THE Angle $\theta_B = 22.5°$.

| n # | $\hbar\omega_B$ KeV | $L_a$ cm | $I_n/I_1$ | $I_n/I_1$ lim $L \to \infty$ | $I_n/I_1$ with $f^2(\sin\theta/\lambda)$ | $I_n/I_1$ Exp Area |
|---|---|---|---|---|---|---|
| 1 | 5 | 0.023 | 1.0 | 1.0 | 1.0 | 1.0 |
| 2 | 10 | 0.221 | 1.088 | 1.201 | 0.363 | 0.640 |
| 3 | 15 | 0.526 | 0.533 | 0.847 | 0.095 | 0.235 |
| 4 | 20 | 0.979 | 0.275 | 0.665 | 0.035 | 0.078 |

TABLE 14: THEORETICAL AND EXPERIMENTAL VALUES FOR THE INTENSITY OF THE $n^{th}$ ORDER PEAK VS THE n = 1 PEAK AT THE ANGLE $\theta_B = 21.7°$.

| n # | $h\omega_B$ KeV | $L_a$ cm | $I_n/I_1$ | $I_n/I_1$ lim $L \to \infty$ | $I_n/I_1$ with $f^2(\sin\theta/\lambda)$ | $I_n/I_1$ Exp Area |
|---|---|---|---|---|---|---|
| 1 | 5 | 0.023 | 1.0 | 1.0 | 1.0 | 1.0 |
| 2 | 10 | 0.221 | 1.097 | 1.201 | 0.366 | 1.081 |
| 3 | 15 | 0.526 | 0.544 | 0.847 | 0.097 | 0.497 |
| 3 | 20 | 0.979 | 0.282 | 0.665 | 0.036 | 0.198 |
| 5 | 2● | 1.46 | 0.157 | 0.508 | 0.016 | 0.101 |
| 6 | 30 | 1.74 | 0.094 | 0.350 | 0.0083 | 0.051 |

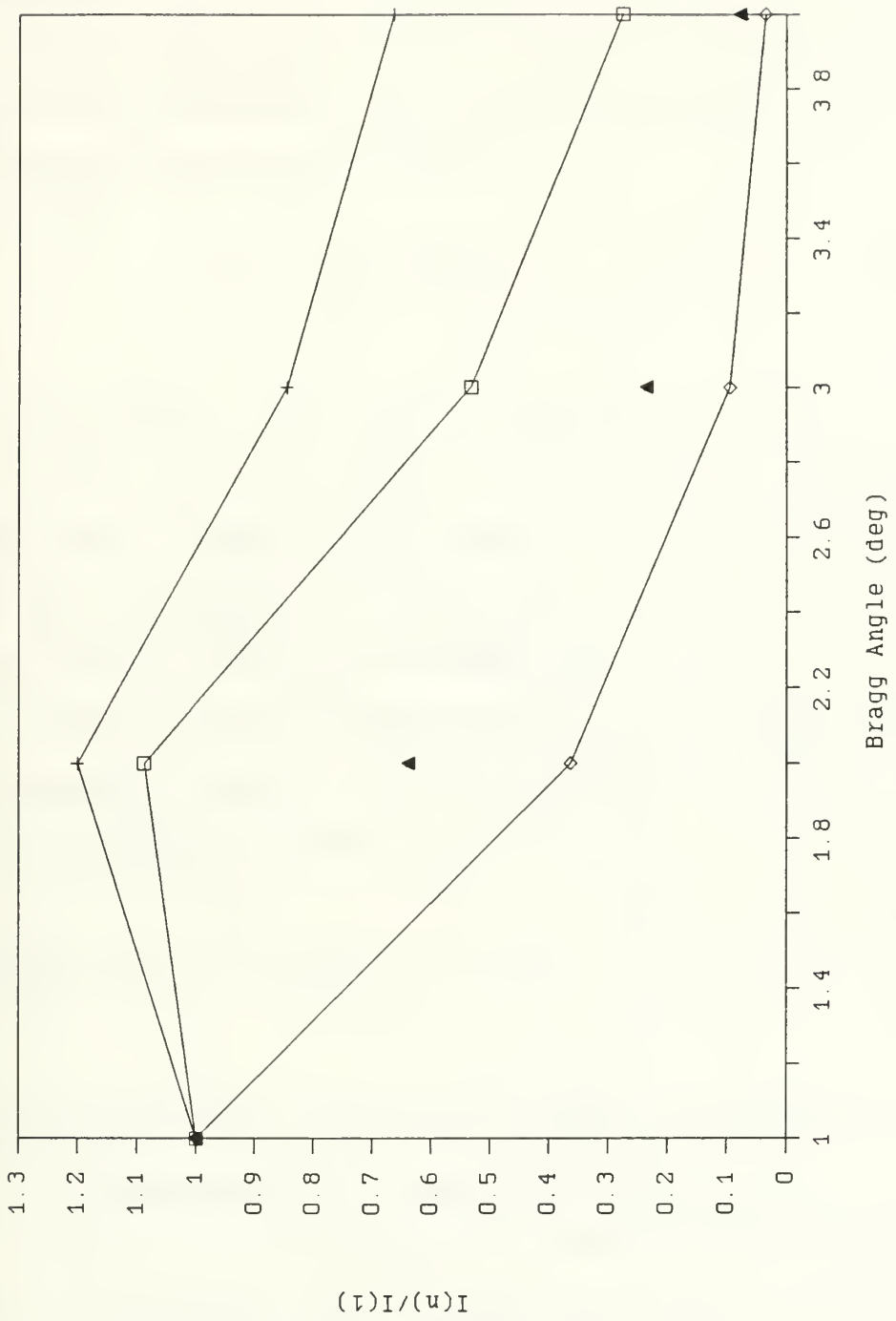


Graph 1: Intensity ratios vs peak number for a Bragg angle of 22.5 degrees.

□ = Equation (24)
+ = Equation (25) lim $L \to \infty$
◇ = Equation (29) $f^2$
▲ = Experiment

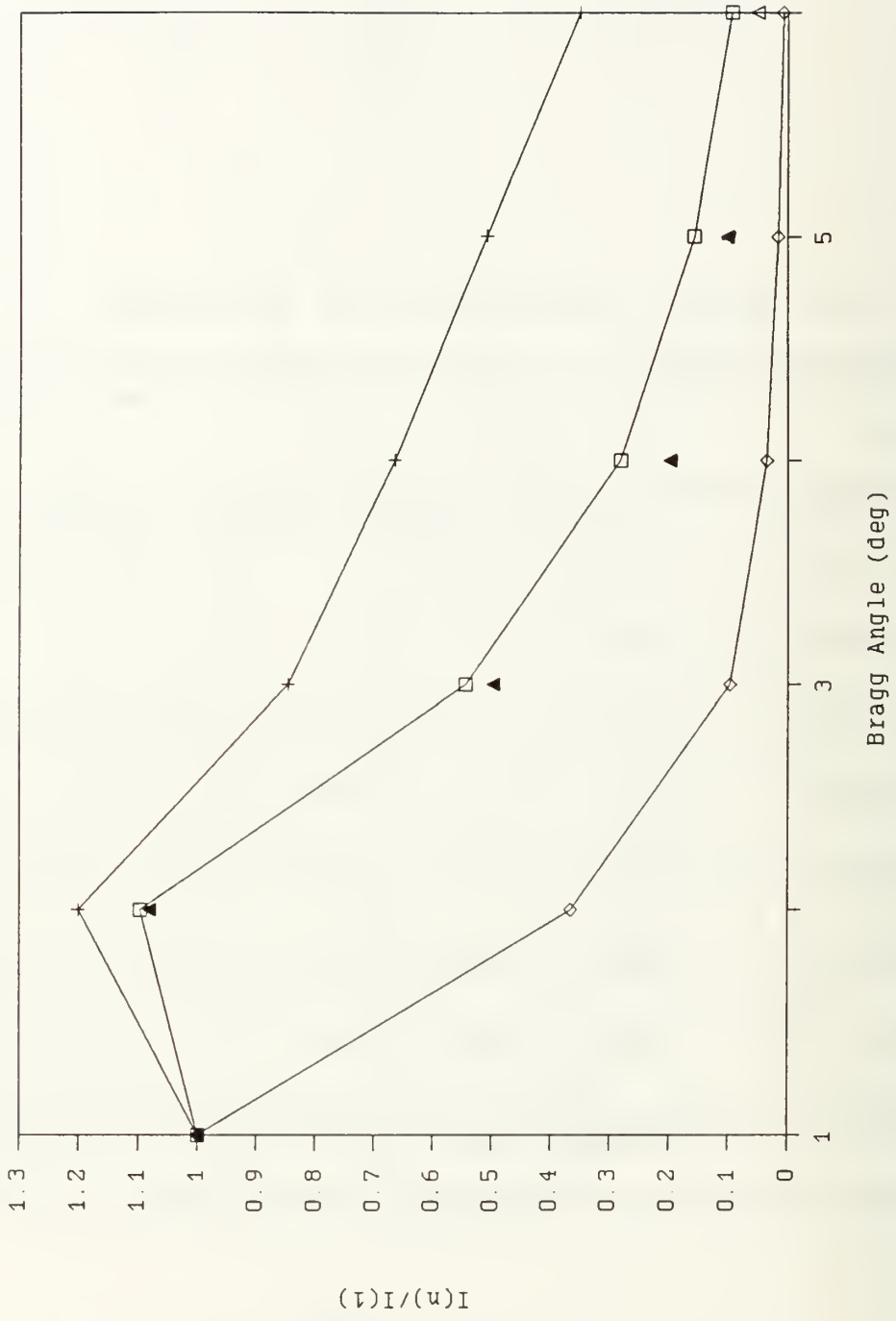


Graph 2: Intensity ratios vs peak number for a Bragg angle of 21.7 degrees and 90 MeV beam.

□ = Equation (24)
+ = Equation (25) $\lim \rightarrow \infty$
◇ = Equation (29) $f^2$
▲ = Experiment

## C. ROCKING DATA

In rotating the mosaic carbon crystal about a nominal Bragg angle of 22.5 degrees, the energy of the peaks vary with the Bragg angle in accordance with;

$$\omega_B = \frac{n\pi c}{d\sin(\theta_B)}. \tag{30}$$

However, this energy relationship to the Bragg angle is only applicable when the measurement by the detector is taken at the Bragg angle. Equation (30) requires that the energy of the PXR will decrease as the Bragg angle is increased. Adishchev et al [Ref. 10] measured the PXR in a silicon crystal with the crystal at a set Bragg angle and the detector rotated through an angle. The relationship of energies when moving the detector is given by:

$$\frac{\omega-\omega_o}{\omega_o} = ctg(\theta_o)\cos(\alpha)\Delta\theta \quad (c=\hbar=1). \tag{31}$$

The energy of PXR with the detector at the reflected Bragg angle is $\omega_o = \pi n/[d\sin(\theta_o)]$ where the angle $\theta_o = \theta_B = \theta_D/2$ and $\theta_d$ is the observation angle with respect to the electron beam line. The angle $\alpha$ is the angle the crystal is tilted from the horizontal plane that the detector and electron beam define. The angle $\Delta\theta$ defines the difference between $\theta_o$ and

$\theta_B$ when the detector is not centered at the Bragg angle. [Ref. 10]

When the detector is stationary and the Bragg angle is varied so that the center of the detector is not at the Bragg angle the energy can be calculated by:

$$\omega = \omega_B \left[ 1 - \frac{\theta_x}{\tan \theta_B} \right] \qquad (32)$$

where $\theta_x$ is the angle from the reflected Bragg angle to the detector [Ref. 7]. The peak energy cones for the PXR with respect to the horizontal plane are located at a peak angle of $\theta_{peak}$ which is equal to $\gamma^{-1}$ = 0.324 degrees = 5.65 milli-radians shown in Figure 15.

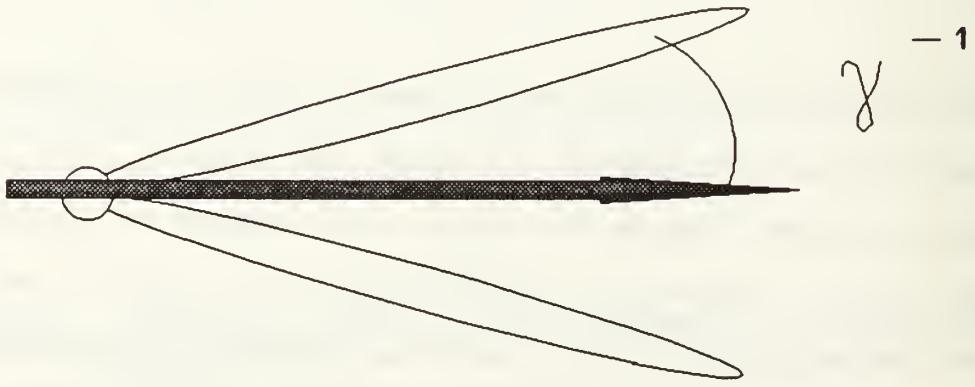


Figure 15: The relationship of the peak cones to $\gamma^{-1}$.

The detector is located 183 cm from the crystal and has a window of 1 cm by 1 cm resulting in a detector half angle of $\theta_d$ = 0.207 degrees. The relationship of the angles is schematically represented in Figure 16, where it is shown that the detector does not include the peak angle for the PXR resulting in the change of energy due to displacement of the detector from the Bragg angle.

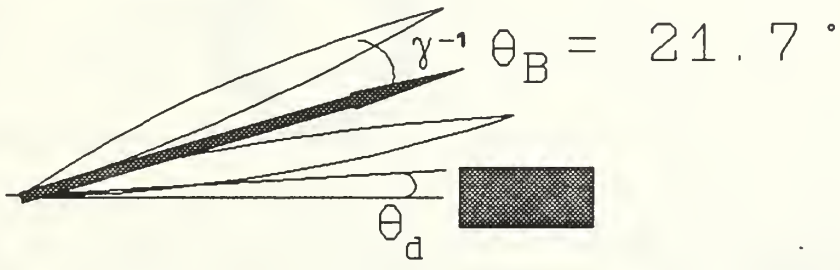


Figure 16: The relationship of the detector half angle $\theta_d$ to the peak cone locations for the PXR.

The energy for the first order peaks, both theoretical and experimental, is plotted in Graph 3 and tabulated in Table 15. The energy associated with the Bragg angle change increases as the Bragg angle decreases. The distribution of the intensities are related to the position the detector is located from the center of the PXR. The distribution variables for the intensities $\theta_x$ and $\theta_y$ are shown in Figure 17. The energy associated with the displacement of the detector in the $\theta_x$ axis falls off as the Bragg angle decreases. The horizontal distribution $\theta_x$ accounts for the

displacement energy change as the detector is rotated, while the vertical $\theta_y$ energy should follow the Bragg formula. The average of the Bragg and displacement variations is plotted on Graph 3. The experimental energy levels are plotted alongside the theoretical values. The experimental value at the Bragg

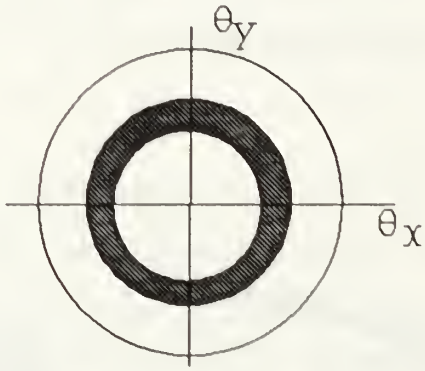


Figure 17: The relationship of $\theta_x$ and $\theta_y$ to the center of the PXR.

angle of 22.5 degrees is higher than the theoretical values, this may be attributed to the uncertainties in the titanium-copper calibration of the PA program. Also the exact proportions of the distributions $\theta_x$ and $\theta_y$ may be different than a one to one ratio that was utilized. The experimental values follow the average value of the Bragg and the displacement values at the smaller angles, however they then follow the trend of the displacement values at larger angles. Graph 4 shows the relationship of the Bragg angle to the intensity ratios for each peak. The uncertainties of the peaks at the angles furthest from the Bragg angle rise

appreciably due to the amount of data taken. The FWHM for these angles are about 500 eV, which if applied to the larger angles can account for the variation from the average theoretical values. The peaks at $\theta_B$ = 21.5 degrees have higher acquisition rates than the center Bragg angle of 22.5 degrees as shown in Graph 5. This could suggest that the conjecture formulated previously about the PXR reflecting off the three foot copper port may be correct. The counts per second rate is higher at an incident Bragg angle of 21.5 degrees than at any other angle. The drastic fall off on either side indicates that the peak cones in the $\theta_x$ direction might be reflected more directly into the detector than any other angle. Again the suggestion of a further experiment with a small or collimated detector located close to the scattering chamber is brought forward. This arrangement would preclude the reflection off the sides of the three foot port.

TABLE 15: THE FIRST ORDER PEAK X-RAY ENERGIES FOR MOSAIC CRYSTAL <002> WITH 90 MeV ELECTRON BEAM.

| Bragg Angle $\theta_B$ | Bragg Theory Energy (KeV) | Disp Theory Energy (KeV) | Average of Theory (KeV) | Exp Value Energy (KeV) |
|---|---|---|---|---|
| 19.0° | 5.67 | 3.66 | 4.67 | 4.68 |
| 20.0° | 5.40 | 4.10 | 4.75 | 4.68 |
| 21.0° | 5.15 | 4.45 | 4.80 | 4.69 |
| 21.5° | 5.04 | 4.59 | 4.82 | 4.85 |
| 22.0° | 4.93 | 4.72 | 4.82 | 4.93 |
| 22.5° | 4.83 | 4.83 | 4.83 | 4.94 |
| 23.0° | 4.73 | 4.93 | 4.83 | 5.05 |
| 24.0° | 4.54 | 5.08 | 4.81 | 5.20 |

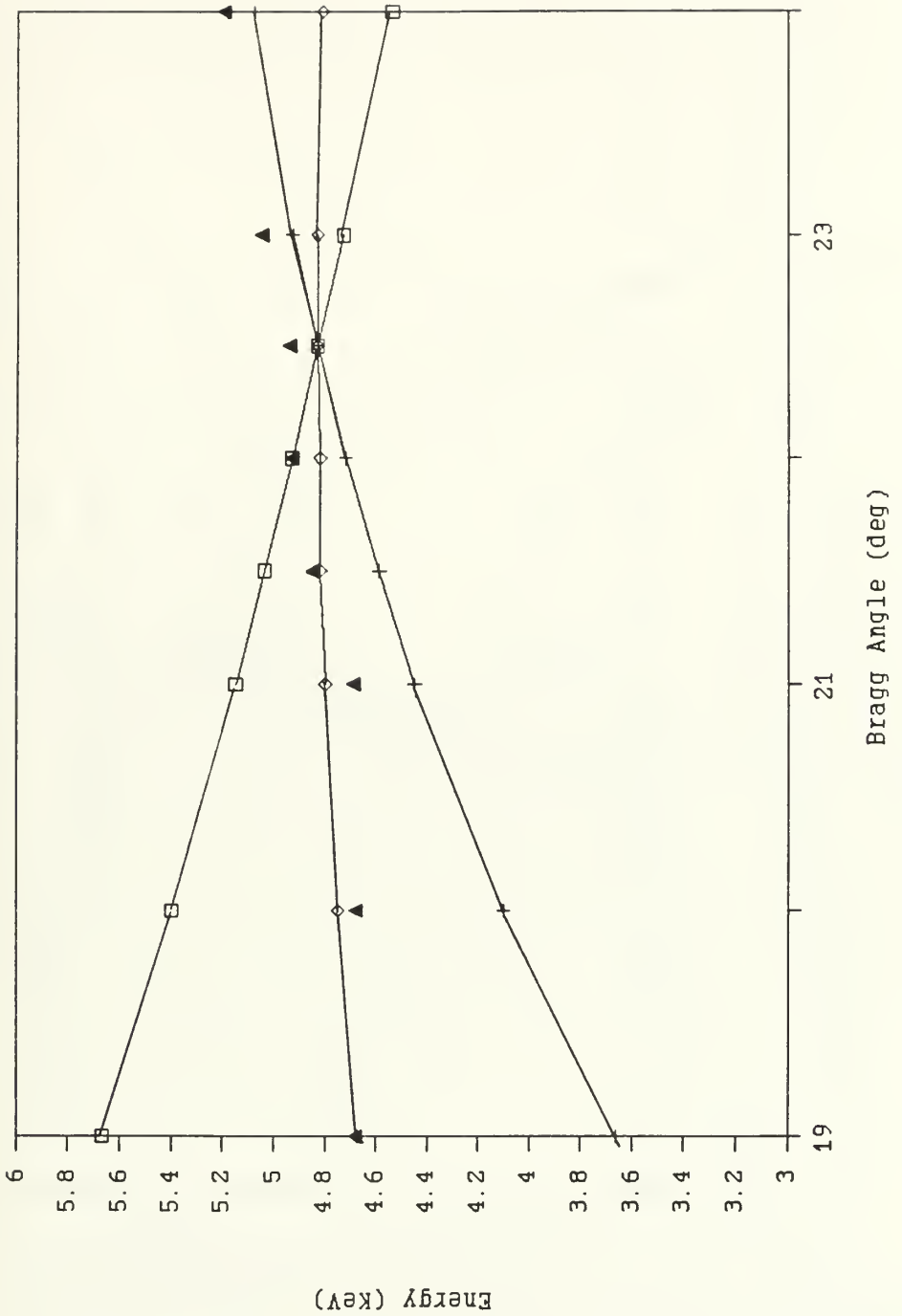


Graph 3: Energy (KeV) of mosaic carbon crystal first order peaks for 90 MeV electron beam vs Bragg angle (deg).

▫ = Bragg Theory

\+ = Displacement Theory

◇ = Average of Bragg and Displacement Theory

▲ = Experimental Data

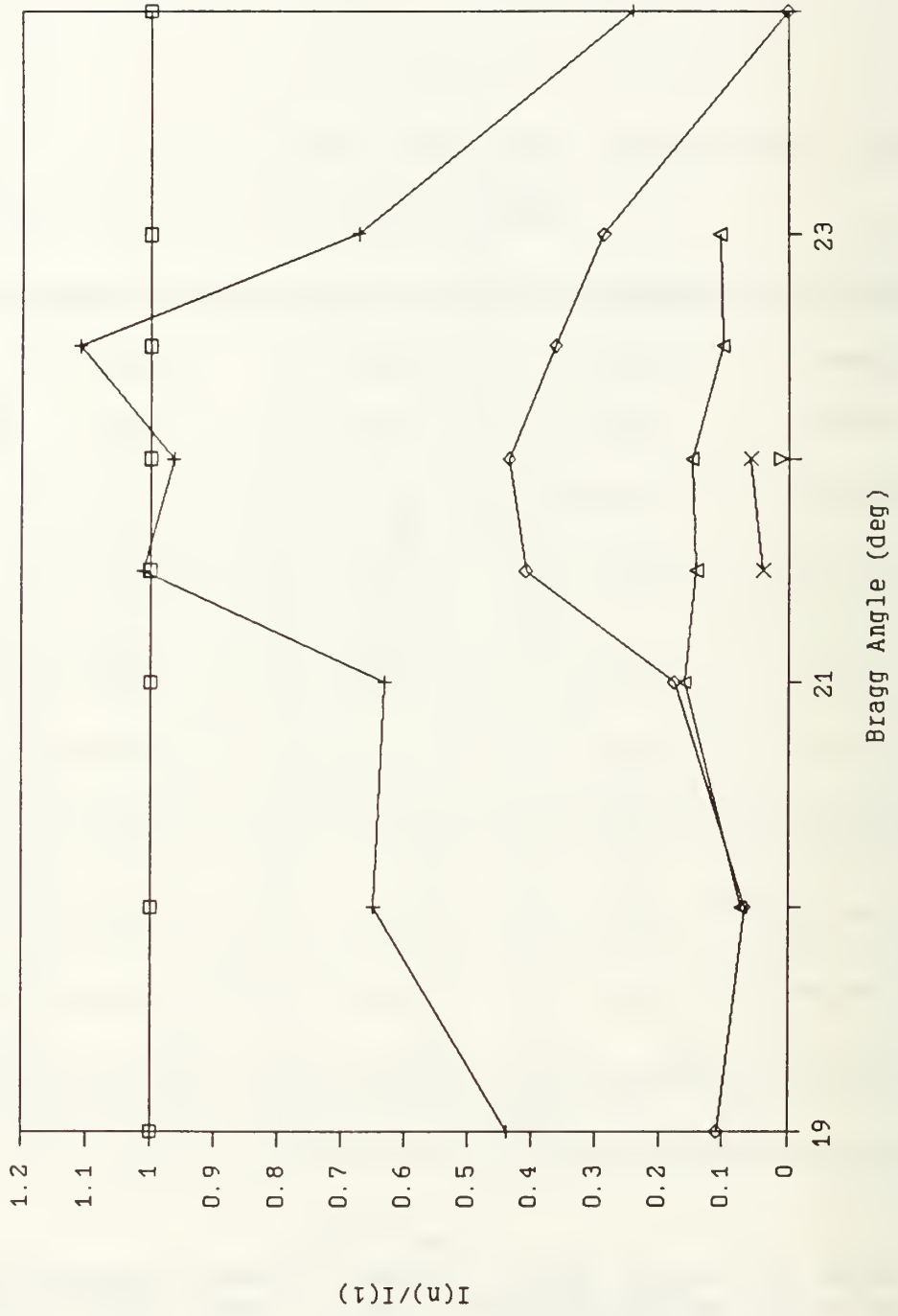


Graph 4: Peak area intensity ratios I(n)/I(1) for each Bragg angle and a 90 MeV beam.

□ = First Peak + = Second Peak ◇ = Third Peak
△ = Fourth Peak x = Fifth Peak ▽ = Sixth Peak

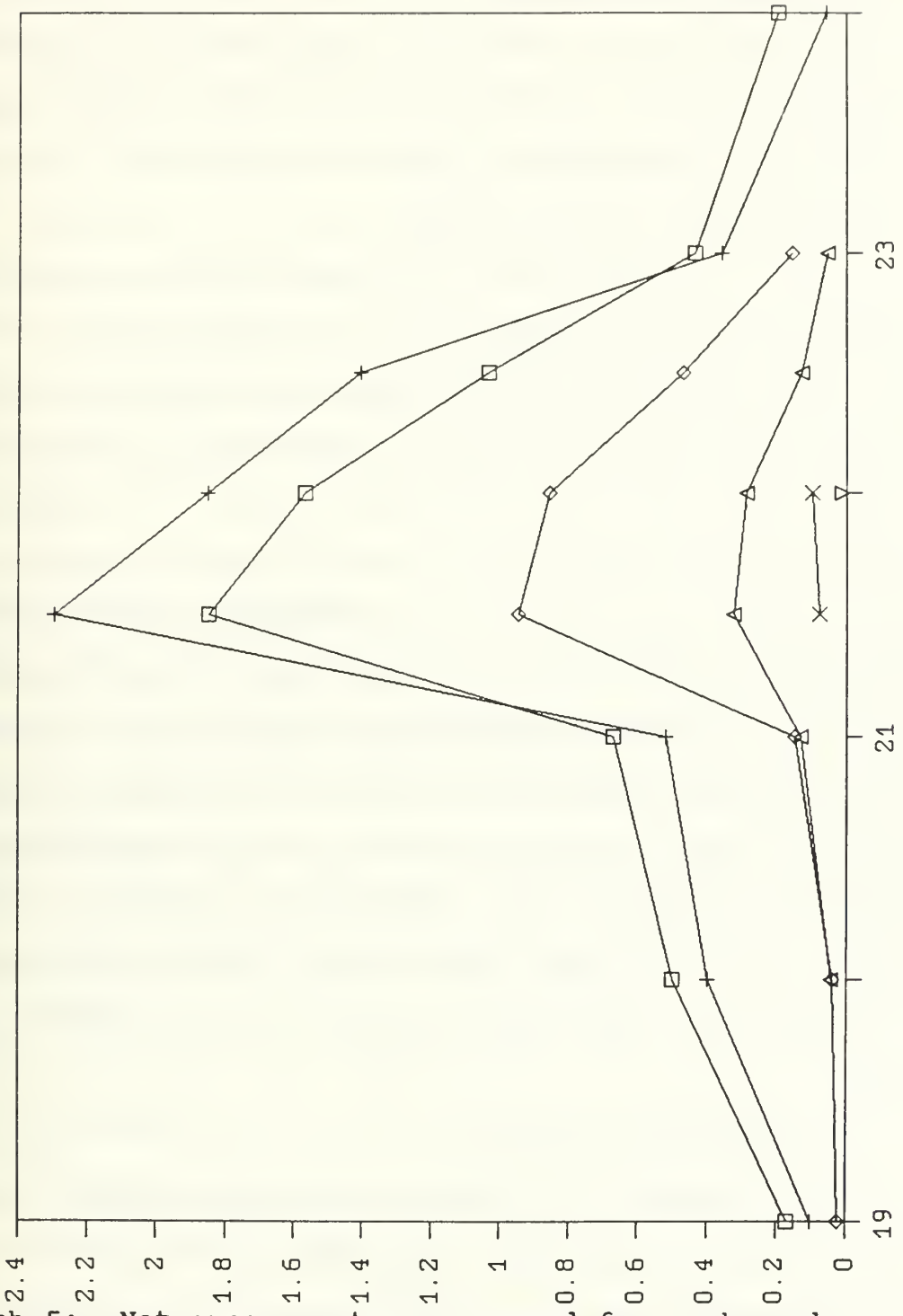


Graph 5: Net area counts per second for each peak vs the incident Bragg angle.

□ = First Peak + = Second Peak ◇ = Third Peak

△ = Fourth Peak x = Fifth Peak ▽ = Sixth Peak

## D. PXR EXPERIMENTAL SETUP

The experimental setup for the parametric x-radiation (PXR) measurements consisted of aligning the reference laser, installation and alignment of the data acquisition equipment.

### 1. Reference Laser Alignment

The reference laser was aligned through a port in the scattering chamber perpendicular to the path of the electron beam. This was accomplished using the geometric centers of that port and the port located perpendicular to the beam on the opposite side of the scattering chamber. Once the laser was leveled and propagating through the geometric centers, the target ladder was raised to put the pinhole in the center of the phosphorescent screen at the electron beam height to verify that the beam passed through the pinhole. The height of the laser beam was also verified by referencing the beam to a point previously marked on the wall of the room housing the scattering chamber. The ladder was rotated 22.5 and 45 degrees with the target ladder height set at the mirror to verify that the laser beam centered on the 45 and 90 degree ports.

### 2. Acquisition Equipment

The detector utilized for data acquisition of the PXR is a silicon lithium (SiLi) detector cooled with a liquid nitrogen dewar. The SiLi detector dewar size required that a three foot extension port be manufactured. This port is

manufactured of brass with a three centimeter diameter window consisting of one mil kapton. The dewar was also required to isolated from ground to prevent noise spikes in the SiLi detector. The sensor of the SiLi detector was positioned three centimeters from the kapton window. This arrangement minimizes the attenuation of the x-radiation.

The Nucleus Personal Computer Analyzer (PCA) card provided the interface between the SiLi detector and the IBM compatible computer for the pulse height analysis (PHA) operation.

**E. LINAC TUNEUP PROCEDURE**

The NPS linear accelerator is a product of the 1960's technology and is primarily designed for radiation and nuclear structure studies. The linac is a three stage, pulsed, S-band RF accelerator with an energy from 20-100 MeV and average currents of about 0.5 microampere. The beam pulse duration is about one microsecond and the pulse repetition rate is 60 Hz. Simply described, electrons, generated by an electron gun similar to a TV, are accelerated, the electron beam is deflected by magnets into the main scattering chamber.... The control room has the control equipment for the acceleration of the electrons and to steer the beam into the target areas. [Ref 11]

The procedure to tune up the NPS linac must be adhered to on every occasion the linac is used to ensure the highest

quality beam. The linac energy is set with deflection magnets adjusted to ensure the electron beam arrives at the scattering chamber. Once maximum current is obtained, the focusing quadrupoles located just prior to the scattering chamber are used to focus the electron beam at the target ladder. The steering magnets, located prior to the deflection magnets, are then adjusted to center the beam in the magnetic field of the focusing quadrupole magnets. This is accomplished by rocking the control for the horizontal steering magnets back and forth and observing the electron beam at the target ladder by remote camera. As the control is rocked the focused beam will spread out symmetrically if the beam is centered in the focusing quadrupole. If the beam is not centered the electron beam at the target ladder will drift necessitating an adjustment of upstream magnets. Once the horizontal positioning is correct the vertical position is verified in the same manner. The position of the electron beam is then verified to be in the geometric center of the focusing quadrupole by turning off the focusing magnets. If the electron beam at the target drifts the beam must then be repositioned. These steps are repeated until the electron beam is centered in both the magnetic and geometric center of the quadrupole magnets.

## F. PULSE HEIGHT ANALYSIS PROCEDURE

Pulse height analysis is energy calibrated using copper and titanium foil strips. The strips are superglued to the

back of the lower half of the phosphorescent screen on the target ladder. The electron beam is directed through the strips and the SiLi detector acquires data for the Nucleus PHA program indicating the associated peak channels for the given source. These peak channels will enable the later conversion of the PXR channels acquired to the energy of the x-radiation by the following equations:

$$E_{exp} = ( \alpha \times Ch_{exp}^{peak} ) - \beta \quad (32)$$

$$\alpha = \frac{E_{Ti} - E_{Cu}}{Ch_{Ti}^{peak} - Ch_{Cu}^{peak}} \quad (33)$$

$$\beta = E_{Cu} - ( \alpha \times Ch_{Cu}^{peak} ) \quad (34)$$

where E is the energy, Ch is the peak channel, $\alpha$ is the slope and ß is the intercept of the energy vs channels linear plot associated with the PHA program. [Ref. 12]

The PHA program is able to plot the occurrence of a parametric x-ray striking the SiLi detector in a relationship of number of activations vs energy.

## V. CONCLUSION AND RECOMMENDATIONS

The ability to measure higher order PXR from a low energy, 90 MeV, electron beam has been demonstrated. The enhancements of the higher order PXR peaks from the {002} plane of a mosaic carbon crystal using a 90 MeV electron beam have been observed. The relationship of the PXR energy to the Bragg angle with a stationary detector correlated with the theory. These distinct energy peaks that can be calculated prior to the experiment, make it possible to use PXR in many applications where x-radiation of a monochromatic nature derived from a low energy linac is desired. The relationship of the intensity ratios requires further explanation that future experiments can fulfill.

The PXR experiment should be repeated in several different varieties. First and foremost in any experiment should be the energy calibration. The calibration should have sufficient time allowed to collect data to ensure error probability is reduced.

The rotating of the crystal through a range of Bragg angles with a stationary detector should be pursued further. The detector should either be collimated or of sufficient distance from the crystal to reduce the detector half angle. Further studies in this field could lead to being able to produce desired energies that may not have been possible due

to physical system constraints. The possibility of having a collimated detector at a short distance from the crystal could lead to studying the detector displacement energy shift. A linear array detector that can determine energies at each step could provide valuable insight into this phenomena.

The field of PXR has been studied intensively in the Soviet Union, however this exciting field of x-radiation production has not been actively pursued elsewhere. PXR can provide many benefits and should be researched further to exploit its potential.

# APPENDIX

The Easy-Mover program is a user friendly program that utilizes quick basic. The program is menu driven with the user choosing the desired menu item by pressing the number associated with the desired function. The program is designed to be used with the PCX board that is installed as a motor controller for the NPS linac target ladder. The program is designed to control three axes of movement that are necessary for ladder movement. The program can easily be programmed to include one more axis of movement which is the limit for the PCX board.

## A. INITIAL SUBROUTINE

The initial subroutine can not be modified by the user once the program has been initiated. If the user desires to change the initial settings, the quick basic program must be entered. The user must call up the easy.bas routine and edit the routine and then save the desired changes.

The initial settings are for accelerations of 1000 steps per sec $^2$ and velocities of 200 steps per sec. The sinusoidal acceleration curve was chosen to reduce backlash and uncertainties in final movement position.

## B. MAIN SCREEN

The main screen gives the user a choice of options that can be selected by pressing the associated number to the desired option. The main screen does not offer any movement options. The main screen provides the user with the ability to choose the subscreen desired. The options available from the main screen are:

- 1. Interactive Routine.
- 2. Rotation Routine.
- 3. Tilt Routine.
- 4. Height Routine.
- 5. Exit Program.

The interactive routine enables the user to type commands directly to the PCX board. The rotation, tilt and height routines transfer the user to the subscreen chosen.

## C. ROTATION SUBSCREEN

The rotation subroutine is utilized for PCX x axis movement which rotates the ladder about a vertical axis. The options available in the rotation subscreen are:

- 1. Home Routine.
- 2. CW Rotation.
- 3. CCW Rotation.
- 4. Zero Counter.
- 5. Change Velocity.
- 6. Return Main.

The home routine provides the user with the ability to find home which is associated with the reference laser. The reference laser and the home detector diodes must be on for the home routine to work. Once the user chooses the home routine, the enter key must be depressed to initiate the routine. The movement of the ladder can be verified both by seeing "Going Home!" on the screen appear and by the remote camera monitoring the ladder position. When operating the home routine the user must observe the reference laser and target ladder monitors to ensure the home routine is operating properly. If necessary the user can depress the "s" key to stop the routine. The home routine will overshoot the home position and then single step back to the home position to enable accurate positioning.

The CW and the CCW routines provide for counter-clockwise and clockwise movement respectfully of the ladder about the vertical axis. These rotation routines are calibrated for degrees. If a ladder with a tilt goniometer is utilized care must be taken to prevent wrapping the control cable around the ladder. Pressing the "s" key will stop movement and return the user to the main screen, while pressing the space bar will enable the interactive program.

The zero counter routine enables the user to define a reference angle for the x axis and designate that angle zero degrees. The PCX board internal position counter is zeroed also. If the home routine is utilized again, the reference

laser will be designated the zero position by the home routine.

The change velocity routine changes the x axis velocity to the input number of steps per second. The initial setting for the x axis velocity is 200 steps per second.

The return main routine returns the user to the main screen.

**D. TILT SUBSCREEN**

The tilt subroutine is utilized for PCX y axis movement which rotates the upper target on the ladder about a vertical axis. The options available to the user in the tilt subscreen are:

- 1. Forward Tilt.
- 2. Backward Tilt.
- 3. Zero Counter.
- 4. Change Velocity.
- 5. Return Main Menu.

The forward and backward tilt routines provide for rotation of the uppermost target on the ladder about the horizontal axis. These tilt routines rotate a goniometer attached to the uppermost target at one motor step per value input. Pressing the "s" key will stop movement and return the user to the main screen, while pressing the space bar will enable the interactive program.

The zero counter routine enables the user to define a reference angle for the tilt axis and designate that position zero degrees. The PCX board internal position counter is zeroed for the y axis also.

The change velocity routine changes the y axis velocity to the input number of steps per second. The initial setting for the y axis velocity is 200 steps per second.

The return main routine returns the user to the main screen.

**E. HEIGHT SUBSCREEN**

The height subroutine is utilized for PCX z axis movement which raises and lowers the ladder. The options available to the user in the height subscreen are:

- 1. Raise Ladder.
- 2. Lower Ladder.
- 3. Zero Counter.
- 4. Change Velocity.
- 5. Return Main Menu.

The forward and backward tilt routines provide for rotation of the uppermost target on the ladder about the horizontal axis. These tilt routines rotate a goniometer attached to the uppermost target at one motor step per value input. Pressing the "s" key will stop movement and return the

user to the main screen, while pressing the space bar will enable the interactive program.

The zero counter routine enables the user to define a reference angle for the ladder height and designate that position zero. The PCX board internal position counter is zeroed for the z axis.

The change velocity routine changes the z axis velocity to the input number of steps per second. The initial setting for the y axis velocity is 200 steps per second.

The return main routine returns the user to the main screen.

**F. INTERACTIVE PROGRAM**

The interactive program enables the user to program the PCX board directly from the keyboard. When the interactive routine is chosen from a movement command by pressing the space key the user can determine position of the ladder by utilizing the "rp" command. This command will give the current position of the stepper motor in steps, the user must convert those steps to whichever unit he is using. The interactive mode enables the user to enter any PCX program command from the PCX board owners manual. To exit the PCX board, the user must depress control-c.

## G. EASY-MOVER COMPUTER PROGRAM

The Easy-Mover program is written in quick basic to operate the stepper motors for height, rotation, and tilt of the target ladder. Incorporated in the Easy-Mover program are pieces of code from the example basic program included with the PCX board. The Easy-Mover program is as follows:

- The subroutines are declared with their parameters.

```
DECLARE SUB checkstatus (status!)
DECLARE FUNCTION readpcxdata! ()
DECLARE SUB writepcxdata (outletter!)
```

- The input/output addresses for the PCX board are defined.

```
CONST DATAREG = 768, DONEREG = 769, CONTROLREG = 770
CONST STATUSREG = 771
```

- The flag bits for the status register are defined.

```
CONST DONEBIT = 16, IBFBIT = 32, TBEBIT = 64, IRQBIT = 128
CONST CMDERRBIT = 1, INITBIT = 2, ENCBIT = 4, OVRTBIT = 8
```

- The initial conditions are set in the subroutine initial.
- The number of steps per unit of axis movement is set by xstep#, ystep# and zstep#.
- The acceleration is set to a sinusoidal acceleration curve by "cn".

```
Initial:

    xstep# = 213.4314#
```

```
    ystep# = 1#

    zstep# = 0.0#

    GOSUB ic

    CMD$ = " ax ac1000 vl200 cn "

    GOSUB Readcommand

    CMD$ = " ay ac1000 vl200 cn "

    GOSUB Readcommand

    CMD$ = " az ac1000 vl200 cn "

    GOSUB Readcommand

    GOSUB Xzero

    GOSUB Yzero

    GOSUB Zzero

    position$ = ""

    exitall = false
```

- The choice of axis movement is made in the Main subroutine which displays the choices on the computer screen.
- The Main subroutine will stay in the Main subroutine until the appropriate key is depressed.
- The x axis provides rotational movement, while the y axis provides for tilt and the z axis provides for height movement.

```
Main:

    colorA = 7

    colorB = 9

    GOSUB Vscreen

    LOCATE 14, 5:  PRINT "1.  Interactive Routine"

    LOCATE 15, 5:  PRINT "2.  Rotation Routine"
```

```
    LOCATE 16, 5:  PRINT "3.  Tilt Routine"
    LOCATE 17, 5:  PRINT "4.  Height Routine"
    LOCATE 18, 5:  PRINT "5.  Exit Program"
    GOSUB Posit
    DO
        ch$ = INKEY$
        LOOP WHILE ch$ = ""
        chval = VAL(ch$)
        IF chval > 0 AND chval < 5 THEN
            GOSUB K1
            ON chval GOSUB Inter, Rotate, Tilt, Height, Quit
        END IF
    GOSUB Main
```

- The Rotate subroutine operates the x axis and rotates the target ladder around a vertical axis.

```
Rotate:
    colorA = 13
    colorB = 5
    GOSUB Vscreen
    LOCATE 10, 32:  PRINT "Rotation Routine"
    LOCATE 14, 5:  PRINT "1.  Home Routine"
    LOCATE 15, 5:  PRINT "2.  CW Rotation"
    LOCATE 16, 5:  PRINT "3.  CCW Rotation"
    LOCATE 17, 5:  PRINT "4.  Zero Counter"
    LOCATE 18, 5:  PRINT "5.  Change Velocity"
```

```
    LOCATE 19, 5:  PRINT "6.  Return Main"
    GOSUB Posit
    DO
        ch$ = INKEY$
        LOOP WHILE ch$ = ""
        chval = VAL(ch$)
        IF chval > 0 AND chval < 7 THEN
            GOSUB Kl
            ON chval GOSUB Hm, Cw, Ccw, Xzero, Xcv, Main
        END IF
    GOSUB Rotate
```

- The Tilt subroutine operates the y axis and rotates the upper most target on the target ladder about a horizontal axis.

```
Tilt:
    colorA = 2
    colorB = 6
    GOSUB Vscreen
    LOCATE 10, 34:  PRINT "Tilt Routine"
    LOCATE 14, 5:  PRINT "1.  Forward Tilt"
    LOCATE 15, 5:  PRINT "2.  Backward Tilt"
    LOCATE 16, 5:  PRINT "3.  Zero Counter"
    LOCATE 17, 5:  PRINT "4.  Change Velocity"
    LOCATE 18, 5:  PRINT "5.  Return Main Menu"
    GOSUB Posit
    DO
```

```
        ch$ = INKEY$
        LOOP WHILE ch$ = ""
        chval = VAL(ch$)
        IF chval > 0 AND chval < 6 THEN
            GOSUB K1
            ON chval GOSUB Forward, Backward, Yzero, Ycv,
Main
        END IF
    GOSUB Tilt
```

- The Height subroutine operates the z axis and raises and lowers the ladder.

```
Height:
    colorA = 4
    colorB = 8
    GOSUB Vscreen
    LOCATE 10, 32: PRINT "Ladder Height Routine"
    LOCATE 14, 5:  PRINT "1.  Raise Ladder"
    LOCATE 15, 5:  PRINT "2.  Lower Ladder"
    LOCATE 16, 5:  PRINT "3.  Zero Counter"
    LOCATE 17, 5:  PRINT "4.  Change Velocity"
    LOCATE 18, 5:  PRINT "5.  Return Main Menu"
    GOSUB Posit
    DO
        ch$ = INKEY$
        LOOP WHILE ch$ = ""
```

```
        chval = VAL(ch$)
        IF chval > 0 AND chval < 6 THEN
            GOSUB Kl
            ON chval GOSUB Raise, Lower, Zzero, Zcv, Main
        END IF
    GOSUB Height
```

- The Vscreen subroutine makes the background for the Main, Rotate, Tilt, and Elevate subroutines.

```
Vscreen:
    GOSUB clearibf
    GOSUB kl
    CLS
    SCREEN 9
    LINE (0, 0) - (630, 330), , B
    PAINT (100, 100), colorA, 15
    LINE (100,45) - (520, 140), , B
    PAINT (200, 130), colorB, 15
    LINE (175, 65) - (455, 120), 0, B
    PAINT (200, 80), 0
    LINE (20, 175) - (275, 325), 0, B
    PAINT (150, 200), 0
    LOCATE 6, 34
    PRINT "EASY-MOVER"
    LOCATE 8, 25
    PRINT "STEPPER MOTION CONTROL SOFTWARE"
```

```
    RETURN
```

- Posit subroutine displays the current position of the axes.

```
Posit:

    LOCATE 19, 37:  PRINT " Current Angle => "

    LOCATE 19, 58:  PRINT currentangle#

    LOCATE 20, 37:  PRINT " Tilt Angle    => "

    LOCATE 20, 58:  PRINT tiltangle#

    LOCATE 21, 37:  PRINT " Height        => "

    LOCATE 21, 58:  PRINT height#

    RETURN
```

- The Hm routine returns the x axis to the home position utilizing the reference laser.

```
Hm:

    GOSUB Hmscrn

    CMD$ = "ax vl700 "

    GOSUB Readcommand

    LOCATE 15, 30

    PRINT "Searching for HOME!"

    CMD$ = "ax bl0 hh bh3 hm100 bl3 ma100 go "

    GOSUB Readcommand

    SLEEP 1

    CMD$ = "ax bh3 mr700 go"

    GOSUB Readcommand

    CMD$ = "ax vl100 "
```

```
    GOSUB Readcommand
    GOSUB Ic
    SLEEP 1
    CMD$ = "ax bl3 bl0 ws13 mo wt5 wd id "
    GOSUB Readcommand
    GOSUB Ic
    GOSUB Finished
    GOSUB Kl
    GOSUB Xturnoff
    CMD$ = "ax vl200 lp0 "
    GOSUB Readcommand
    currentangle# = 0
    RETURN Rotate
```

- The Cw subroutine provides for clockwise movement of the x axis.

```
Cw:
    GOSUB Kl
    CMD$ = "ax bh3 "
    GOSUB Readcommand
    GOSUB Ic
    GOSUB Cwscrn
    xyzstep# = xstep#
    dir$ = "ax bl0 "
    GOSUB Degree
    GOSUB Finished
```

```
    GOSUB Xturnoff

    currentangle# = currentangle# - DEG#

    RETURN Rotate
```

- The Ccw subroutine provides for counter-clockwise movement of the x axis.

```
Ccw:

    GOSUB Kl

    CMD$ = "ax bl3 "

    GOSUB Readcommand

    GOSUB Ic

    GOSUB Scrnccw

    xyzstep# = xstep#

    dir$ = "ax bl0 "

    GOSUB Degree

    GOSUB Finished

    GOSUB Xturnoff

    currentangle# = currentangle# + DEG#

    RETURN Rotate
```

- The Forward subroutine provides for the forward rotation of the y axis.

```
Forward:

    GOSUB Kl

    CMD$ = "ay bh3 "

    GOSUB Readcommand

    GOSUB Ic
```

```
    GOSUB Scrnforward

    xyzstep# = ystep#

    dir$ = "ay bl2 "

    GOSUB Degree

    GOSUB Finished

    GOSUB Yturnoff

    tiltangle# = tiltangle# - DEG#

    RETURN Tilt
```

- The Backward subroutine provides for the backward rotation of the y axis.

```
Backward:

    GOSUB Kl

    CMD$ = "ay bl3 "

    GOSUB Readcommand

    GOSUB Ic

    GOSUB Scrnbackward

    xyzstep# = ystep#

    dir$ = "ay bl2 "

    GOSUB Degree

    GOSUB Finished

    GOSUB Yturnoff

    tiltangle# = tiltangle# + DEG#

    RETURN Tilt
```

- The Raise subroutine provides for raising the height of the target ladder utilizing the z axis.

```
Raise:
    GOSUB K1
    CMD$ = "az b13 "
    GOSUB Readcommand
    GOSUB Ic
    xyzstep# = zstep#
    dir$ = "az b14 "
    GOSUB Degree
    GOSUB Finished
    GOSUB Zturnoff
    elevation# = elevation# + DEG#
    RETURN Height
```

- The Lower subroutine provides for the lowering of the target ladder utilizing the z axis.

```
Lower:
    GOSUB K1
    CMD$ = "az bh3 "
    GOSUB Readcommand
    GOSUB Ic
    xyzstep# = zstep#
    dir$ = "az b14 "
    GOSUB Degree
    GOSUB Finished
    GOSUB Zturnoff
    elevation# = elevation# - DEG#
```

```
    RETURN Height
```

- The Xzero subroutine zeros the x axis position counters.

```
Xzero:
    CMD$ = "ax lp0 "
    GOSUB Readcommand
    currentangle# = 0
    RETURN
```

- The Yzero subroutine zeros the y axis position counters.

```
Yzero:
    CMD$ = "ay lp0 "
    GOSUB Readcommand
    tiltangle# = 0
    RETURN
```

- The Zzero subroutine zeros the z axis position counters.

```
Zzero:
    CMD$ = "az lp0 "
    GOSUB Readcommand
    elevation# = 0
    RETURN
```

- The Inter subroutine provides for direct user interface with PCX board.
- The user may exit the interactive mode by pressing control-c on the keyboard.

```
Inter:
    CLS
    PRINT "Interactive Mode, Enter PCX command, Press CTRL-C
    to exit!"
    CMD$ = "en wy "
    GOSUB readcommand
    keystroke = 0
    WHILE keystroke <> 3
        key$ = INKEY$
        IF key$ <> "" THEN
            keystroke = ASC(key$)
            writepcxdata (keystroke)
        END IF
        pcxdataout = readpcxdata
        IF (pcxdataout <> 0) AND (pcxdataout <> 10) THEN
            PRINT (CHR$(pcxdataout));
        END IF
        checkstatus (status)
    WEND
    GOSUB Xturnoff
    GOSUB Yturnoff
    gosub Zturnoff
    RETURN Main
```

- The Xcv subroutine lets the user change the x axis velocity from the initial or previous value.

- The Xcv subroutine will not change value of the initial value settings that are set when starting the Easy-Mover program.

```
Xcv:

    Routinename$ = " Change Rotation Velocity "

    GOSUB Cvscrn

    CMD$ = "ax vl" + scrndata$ + " "

    GOSUB Readcommand

    RETURN Rotate
```

- The Ycv subroutine lets the user change the y axis velocity from the initial or previous value.
- The Ycv subroutine will not change value of the initial value settings that are set when starting the Easy-Mover program.

```
Ycv:

    Routinename$ = "  Change Tilt Velocity  "

    GOSUB Cvscrn

    CMD$ = "ay vl" + scrndata$ + " "

    GOSUB Readcommand

    RETURN Tilt
```

- The Zcv subroutine lets the user change the z axis velocity from the initial or previous value.
- The Zcv subroutine will not change value of the initial value settings that are set when starting the Easy-Mover program.

```
Zcv:

    Routinename$ = " Change Height Velocity "
```

```
    GOSUB Cvscrn

    CMD$ = "az vl" + scrndata$ + " "

    GOSUB Readcommand

    RETURN Height
```

- The Kl subroutine executes the PCX kill routine, the command queue is flushed and axis movement stops immediately.

```
Kl:

    CMD$ = "kl "

    GOSUB Readcommand

    RETURN
```

- The Ic subroutine executes the PCX board "ic" command clearing the command queue.

```
Ic:

    CMD$ = "ic "

    GOSUB Readcommand

    RETURN
```

- The Degree subroutine converts the input, scrndata$, to the proper number of steps and executes the axis movement.

```
Degree:

    LOCATE 15, 30

    DEG# = VAL(scrndata$)

    stp# = (xyzstep# * DEG#)

    st# = INT(stp#)

    numsteps$ = STR(st#)
```

```
    chdegree$ = MID$(numsteps$, 2)

    CMD$ = dir$ + "MR" + chdegree$ + " go id "

    GOSUB Readcommand

    RETURN
```

- The Clearibf subroutine clears the pcxdataout buffer so that the PCX board will not freeze up due to a full buffer.

```
Clearibf:

    pcxdataout = 2

    WHILE (pcxdataout <> 0) AND (pcxdataout <>3) AND

    (pcxdataout <> 10)

        pcxdataout = readpcxdata

    WEND

    RETURN
```

- The Xturnoff subroutine disables the current to the x axis motor to prevent overheating.

```
Xturnoff:

    CMD$ = "bh0 "

    GOSUB Readcommand

    RETURN
```

- The Yturnoff subroutine disables the current to the y axis motor to prevent overheating.

```
Yturnoff:

    CMD$ = "bh2 "

    GOSUB Readcommand
```

```
    RETURN
```

- The Zturnoff subroutine disables the current to the z axis motor to prevent overheating.

```
Zturnoff:

    CMD$ = "bh4 "

    GOSUB Readcommand

    RETURN
```

- The Finished subroutine keeps the current screen displayed until the current axis rotation is complete.
- The user may stop axis rotation early by depressing the "s" key.
- The user may enter the interactive routine by depressing the space bar.

```
Finished:

    WHILE exitall = false

        status = INP(STATUSREG)

        IF (status AND DONEBIT) <> 0 THEN

            IF (status AND CMDERRBIT) <> 0 THEN

                CLS

                PRINT "PCX indicates a command error!"

                END

            ELSE

                doneflag = INP(DONEREG)

                IF doneflag <> 0 THEN

                    IF doneflag MOD2 = 1 THEN

                        RETURN
```

```
                END IF
                doneflag = doneflag / 2
                IF doneflag = doneflag MOD 2 = 1 THEN
                      RETURN
                END IF
                doneflag = doneflag / 2
                IF doneflag = doneflag MOD 2 = 1 THEN
                      RETURN
                END IF
             END IF
          END IF
       END IF
       key$ = INKEY$
       IF key$ = " " THEN
          key$ = ""
          GOSUB Inter
       ELSIF key$ = "s" OR key$ = "S" THEN
          key$ = ""
          RETURN
       END IF
    WEND
```

- The Scrn subroutine provides for the displays for axis movement.

```
Scrn:
    SCREEN 9
```

```
    LINE (0, 0) - (630, 330), , B
    PAINT (100, 100), color1, 15
    LINE (100,45) - (520, 140), , B
    PAINT (200,130), color2, 15
    LINE (175, 65) - (455, 120), 0, B
    PAINT (200, 80), 0
    LINE (220, 175) - (415, 225), 0, B
    PAINT (350, 200), 0
    LOCATE 6, 30
    PRINT Routinename$
    LOCATE 8, 30
    PRINT Subname$
    LOCATE 14, 29
    PRINT Name$
    GOSUB Posit
    LOCATE 15, 30
    INPUT scrndata$
    IF scrndata$ = "s" OR scrndata$ ="S" THEN
       GOSUB Main
    END IF
    RETURN
```

- The Hmscrn subroutine initializes the home routine variables for the Scrn subroutine.

```
Hmscrn:
    color1 = 10
```

```
    color2 = 3
    Routinename$ = "   Home Routine"
    Subname$ = ""
    Name$ = "      GOING HOME"
    CLS
    GOSUB Scrn
    currentangle# = 0
    RETURN
```

- The Cwscrn subroutine initializes the clockwise movement routine variables for the Scrn subroutine.

```
Cwscrn:
    color1 = 4
    color2 = 7
    Routinename$ = "Clockwise Movement"
    Subname$ = " Enter # of degrees"
    Name$ = "Degrees"
    CLS
    GOSUB Scrn
    RETURN
```

- The Scrnccw subroutine initializes the counter-clockwise movement routine variables for the Scrn subroutine.

```
Scrnccw:
    color1 = 9
    color2 = 14
    Routinename$ = "     CCW Movement"
```

```
    Subname$ = " Enter # of degrees"
    Name$ = "Degrees"
    CLS
    GOSUB Scrn
    RETURN
```

- The Scrnforward subroutine initializes the forward movement routine variables for the Scrn subroutine.

```
Scrnforward:
    color1 = 7
    color2 = 4
    Routinename$ = " Forward Movement "
    Subname$ = " Enter # of degrees"
    Name$ = "Degrees"
    CLS
    GOSUB Scrn
    RETURN
```

- The Scrnbackward subroutine initializes the backward movement routine variables for the Scrn subroutine.

```
Scrnbackward:
    color1 = 14
    color2 = 9
    Routinename$ = " Backward Movement "
    Subname$ = " Enter # of degrees"
    Name$ = "Degrees"
    CLS
```

```
    GOSUB Scrn
```

- The Scrnraise subroutine initializes the raising movement routine variables for the Scrn subroutine.

```
Scrnraise:

    color1 = 5

    color2 = 3

    Routinename$ = " Raise Target "

    Subname$ = " Enter # of units "

    Name$ = "Units"

    CLS

    GOSUB Scrn

    RETURN
```

- The Scrnlower subroutine initializes the lowering movement routine variables for the Scrn subroutine.

```
Scrnlower:

    color1 = 5

    color2 = 3

    Routinename$ = " Lower Target "

    Subname$ = " Enter # of Units "

    Name$ = "Units"

    CLS

    GOSUB Scrn

    RETURN
```

- The Cvscrn subroutine initializes the change velocity routine variables for the Scrn subroutine.

```
Cvscrn:
    color1 = 9
    color2 = 8
    Subname$ = "Enter Velocity <= 800"
    Name$ = "Velocity"
    CLS
    GOSUB Scrn
    RETURN
```

- The Readcommand subroutine inputs the commands, CMD$, to the PCX board.

```
Readcommand:
    FOR I = 1 TO LEN(CMD$)
        charval = ASC(MID$(CMD$, I, 1))
            WHILE INP(STATUSREG) and TBEBIT = 0
            WEND
        OUT DATAREG, charval
    NEXT I
    GOSUB Command
    RETURN
```

- The Command subroutine checks to see if the PCX board has an error and if so terminates the program.

```
Command:
    status = INP(STATUSREG)
    IF (status and CMDERRBIT) <> 0 THEN
        CLS
```

```
        PRINT "The PCX Board Indicates a Command Error!"
        PRINT "Terminating the Program."
        END
    END IF
    RETURN
```

- The Quit subroutine terminates the program.

```
Quit:
    END
```

- The checkstatus subroutine checks the status of the PCX board.

```
SUB checkstatus (status!)
    IF (status AND DONEBIT) <> 0 THEN
        IF (status AND CMDERRBIT) <> 0 THEN
            PRINT
            PRINT "Command Error!"
        ELSIF (status AND ENCBIT) <> 0 THEN
            PRINT
            PRINT "Encoder Slip Error!"
        ELSIF (status AND OVRTBIT) <> 0 THEN
            PRINT
            PRINT "A limit switch is closed!"
        ELSE
            doneflag = INP(STATUSREG)
            IF doneflag <> 0 THEN
```

```
                PRINT
                PRINT "A DONE flag has been set."
                PRINT "AXES DONE are: ";
                IF doneflag MOD 2 = 1 THEN PRINT "Rotation";
                doneflag = doneflag / 2
                IF doneflag MOD 2 = 1 THEN PRINT "Tilt";
                doneflag = doneflag / 2
                IF doneflag MOD 2 = 1 THEN PRINT "Height";
                doneflag = doneflag / 2
                PRINT "Enter CTRL-Y to clear DONE flags."
            END IF
        END IF
        writepcxdata (24)
    END IF
END SUB 'checkstatus
```

- The function readpcxdata reads the PCX data register.

```
FUNCTION readpcxdata!
    status = INP(STATUSREG)
    IF (status AND IBFBIT) <> 0 THEN
        readpcxdata = INP(DATAREG)
    ELSE
        readpcxdata = 0
    END IF
END FUNCTION 'readpcxdata
```

- The writepcxdata subroutine reads the PCX data register.

```
SUB writepcxdata (outletter)
    While INP(STATUSREG) AND TBEBIT = 0
    WEND
    OUT DATAREG, outletter
END SUB 'writepcxdata
```

## LIST OF REFERENCES


1. Adishchev, Yu.N., and others, "Measurements of Parametric X-Rays from Relativistic Electrons in Silicon Crystals," Nuclear Instruments and Methods in Physics Research, v. B21, pp 49-55, 1987.

2. Baryshevsky, V.G., and others, "Experimental Observation of the Parametric X-Rays from Ultrarelativistic Electrons," J. Physics D: Applied Physics, v. 19, pp 171-176, 1986.

3. Rule, D.W., and others, "Production of X-Rays by the Interaction of Charged Particle Beams with Periodic Structures and Crystalline Materials," paper no. 25 presented at SPIE's International Symposium on Optical Science and Engineering Conf. no. 1552 Short Wavelength Radiation Sources, San Diego, CA, 21-26 July 1991.

4. Faranchuk, I.D., and Ivanshin, A.V., "Theoretical Investigation of the Parametric X-Ray Features," J. Physique, v. T46, no. 11, pp 1981-1986, November 1985.

5. Experiments in Nuclear Science AN34 Laboratory Manual, 3rd ed., Revised, p. 167, EG&G Ortec Incorporated, 1984.

6. Naval Surface Warfare Command, Silver Spring, MD Facsimile Transmission, Rule, D.W. to Maruyama, X.K., Subject: Theoretical Ratios of Intensities for the High Order Reflections (U), 101711Z AUG 91.

7. Interview between D.W. Rule, Naval Surface Warfare Command, Silver Spring, MD, and the author, 13 December 1991.

8. Naval Surface Warfare Command, Silver Spring, MD Facsimile Transmission, Rule D.W. to Maruyama, X.K., Subject: Summary of Comparison Between Experiment and Theory (U), 142056Z NOV 91.

9. Anderson, H.L., and others, A Physicist's Desk Reference the Second Edition of Physics Vade Mecum, p 143, American Institute of Physics, 1989.

10. Adishchev, Yu.N., and others, "Measurements of Spectral and Polarization Characteristics of Parametric X-Rays in a Si Crystal," Nuclear Instruments and Methods in Physics Research, v. B44, pp 130-136, 1989.

11. Hellstern, M.J., Emittance Measurement of the Naval Postgraduate School Linear Accelerator Using Optical Transition Radiation Techniques, Master's Thesis, Naval Postgraduate School, Monterey, CA, September 1991.

12. Interview M.A. Piestrup, Adelphi Technologies Incorporated, Palo Alto, CA, and the author, 5 August 1991.

## INITIAL DISTRIBUTION LIST

No. Copies

1. Defense Technical Information Center.....2
   Cameron Station
   Alexandria, VA 22314-6145

2. Library, Code 52.....2
   Naval Postgraduate School
   Monterey, CA 93943-5002

3. Dr. K. E. Woehler, Code Ph/Wh.....1
   Department of Physics
   Naval Postgraduate School
   Monterey, CA 93943-5002

4. Professor X. K. Maruyama, Code Ph/Mx.....5
   Department of Physics
   Naval Postgraduate School
   Monterey, CA 93943-5002

5. Professor J. R. Neighbours, Code Ph/Nb.....1
   Department of Physics
   Naval Postgraduate School
   Monterey, CA 93943-5002

6. Dr. R. B. Fiorito, Code R41.....1
   Naval Surface Weapons Center
   10901 New Hampshire Avenue
   Silver Spring, MD 20903-5000

7. Dr. D. W. Rule, Code R41.....1
   Naval Surface Weapons Center
   10901 New Hampshire Avenue
   Silver Spring, MD 20903-5000

8. Dr. M. A. Piestrup.....1
   Adelphi Technology Incorporated
   532 Emerson Street
   Palo Alto, CA 94301

9. Mr. D. Snyder, Code 61PH.....1
   Department of Physics
   Naval Post Graduate School
   Monterey, CA 93943-5002